Power Efficiency of the Gyroscopic-Pendulum Wave Energy Converter

A Master of Science thesis by
Sherzad Anwari

T U Delft

Power Efficiency of the Gyroscopic-Pendulum Wave Energy Converter

by

Sherzad Anwari

To obtain the degree of Master of Science
at the Delft University of Technology,
to be defended publicly on Tuesday 29 August, 2019 at 15:00 AM.

Student number: 4176073
Thesis committee: Prof. dr. A. Metrikine, TU Delft, Graduation chairman
Dr. ir. H. Hendrikse, TU Delft, Supervisor
L. M. Masturi, TU Delft, Supervisor

Faculty of Civil Engineering and Geociences
Section Offshore Engineering
Department Hydraulic Engineering

TUDelft

Abstract

The oceans, which cover nearly 70% of the earth's surface, can be considered as an inexhaustible energy source for renewable electricity due to its size and predictability. One way to capture ocean energy is by harnessing the energy produced by waves at sea, by means of devices called wave energy converters (WECs).

Delft University of Technology is developing a new floating WEC concept called the "gyroscopic-pendulum". This concept is a modification of the so called "classical vertical axis pendulum", which is capable of producing mechanical power harvested from the rotations of the pendulum around the vertical axis.

The new concept is proposed by adding a flywheel with the aim to enhance the rotations of the pendulum about the vertical axis. The enhancement comes from gyroscopic precession which is created due to a change in the angular moment of the spinning flywheel caused by the torque originating from the weight of the pendulum.

This thesis starts with a general introduction about wave power followed by the mathematical and numerical model of the gyroscopic-pendulum. Numerical simulations are performed in which the gyroscopic-pendulum and the classical pendulum are both imposed with the same harmonic roll motion, while the gyroscopic-pendulum system also receives some power input to rotate the disk. The main objective is to find out in which ranges of amplitude and frequency of imposed motions, the gyroscopic-pendulum results in an improvement of the power efficiency compared to the classical vertical axis pendulum.

The results obtained from tests performed in the simulated conditions, shows us that the gyroscopic-pendulum has a significantly higher efficiency compared to the classical vertical axis pendulum when the frequency of the imposed roll motion is in the range of 1.4 to 1.75 $\frac{rad}{s}$ and the amplitude is in the range of 0.6 to 0.95 m.

Preface

Before you lies the final report of my master of science thesis, which is necessary to fulfill the graduation requirements of the Offshore & Dredging Engineering program at Delft University of Technology. This report is the result of nine months of research meant to describe the behaviour of a new Wave Energy Converter concept, which is being developed by Delft University of Technology.

It is fair to state that it has been quite a challenging task to perform, but at the same time, or probably due to this reason, it has been a very interesting, educative and fun task to perform. I consider myself lucky to have found this subject together with its assessment committee and achieved all of my personal goals regarding the thesis.

Another fair statement that is necessary to be made in this context is the fact that I would not be able to complete this task without the excellent guidance of my assessment committee.

I would like to express my deepest gratitude for the help and support received from my first supervisor Mamin Masturi. Mamin has invested a lot of his time in me, but always in presence of his calm, patient and friendly personality. I would also like to thank my second supervisor Dr.ir. Hayo Hendrikse for his important contribution to find and understand the correct equations of motions and his help with the interpretations of the results. Many thanks to Prof.dr. Andrei Metrikine for his enlightening guidance through this study and his crucial roll in finding the correct equations of motion. I have always been positively impressed by his great knowledge and his ability to explain and answer every question in a very comprehensible manner.

Since this report will be one of the few things I will personally preserve from my time as a student, let me state something on the personal level. At a very young age, at a far place from here, I had to make a harsh choice between staying in a place I knew everything about or go to some place I didn't know anything about. So I used my imagination to make myself choose for the unknown. It makes me happy to realize that the completion of this degree is one of the successful results of that decision and it makes me full of hope for many more to come. It also makes me realize that reality is just a side effect of the imperfections in our own imagination.

So, finally, a very special recognition goes out to God and my family for their investment, support, patience and encouragement during my life as well as this thesis project.

Sherzad Anwari
Delft, August 2019

Contents

Introduction

1.1. Global Energy Outlook

We have come to an era in which we no longer can deny the importance of the climate change and the accompanied challenges. Due to compelling scientific researches around the world and political shifts focusing more on the well-being of our planet, more attention is given to this phenomenon. The general public, institutions and companies are now also joining the scientist and governments in acknowledging the environmental issues and the importance of a change in the current energy systems. The energy systems of the future must be able to provide for the increasing global energy demand and at the same time tackle the environmental stresses by significantly decreasing the carbon dioxide emissions. In my view this is a very challenging requirement due to the complexity of the global inter-governmental relationships between countries, the complex relationship between governments and the energy industry and for sure due to the complexity of the required technical innovations. These required technical innovations can partially be accounted by the emerging renewable energy systems.

An historical event that really mirrored the acknowledgement of global climate change by the governments was the United Nations Climate Change Conference held in Paris in December of 2015. An universal and legally binding global climate deal was agreed upon by 195 countries, which is now known as the Paris Agreement. The agreement sets out a global action plan to limit the global warming well below 2°C and to limit it to 1.5°C [1]. This would mean that emissions need to be limited between 250 and 450 GtCO2 (gigatonnes CO2) [2] and the energy-related CO2 emission should be around 17.5 GtCO2 [3]. With the energy-related CO2 emission in 2018 being already close to twice of this number (33,1 GtCO2), see Figure 1.1, it will be extremely difficult to achieve the objective(s) of the Paris Agreement.
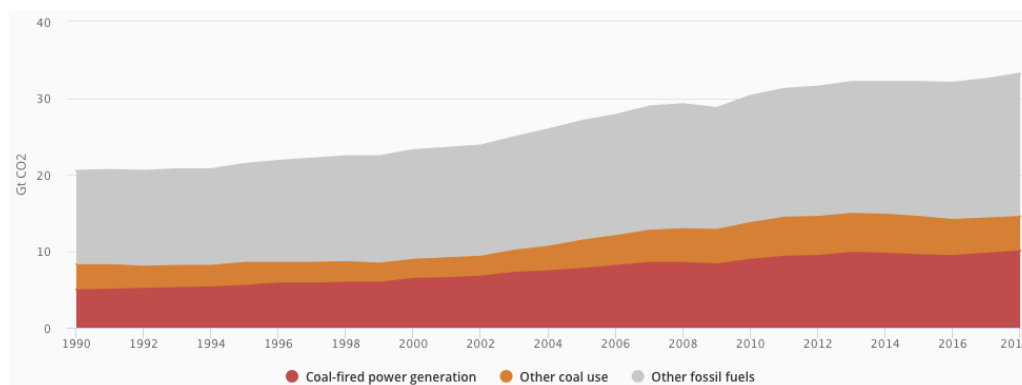
Figure 1.1: Global energy-related carbon dioxide emissions by source, 1990-2018 [3]

The International Energy Agency (IEA), an authoritative and autonomous intergovernmental organization, has come up with three different possible scenarios for the global energy trends: the Current Policies Scenario, the New Policies Scenario and the Sustainable Development Scenario.

The Current Policies Scenario, if there are no changes in policies from today, expects increasing strain on energy security and major rise in energy-related CO2 emissions. The New Policies Scenario, including policies and targets announced by the governments, still does not predict a peak in the energy-related CO2 emissions. The Sustainable Development Scenario, in which accelerated clean energy transition is the key, could put the world on track to meet the climate change goals[3].

It is expected that the economic middle class of the world is likely to expand from 3 billion to more than 5 billion people by 2030, resulting in vastly improved living standards. The improved living standards cause a rise in energy use in many developing countries leading to a 25% rise in the global energy demand in 2030 [4]. This forecast is in line with the New Policies Scenario and thus will not lead to achieving the goals set by the Paris Agreement. Figure1.2 shows us the forecasted energy demand by source.
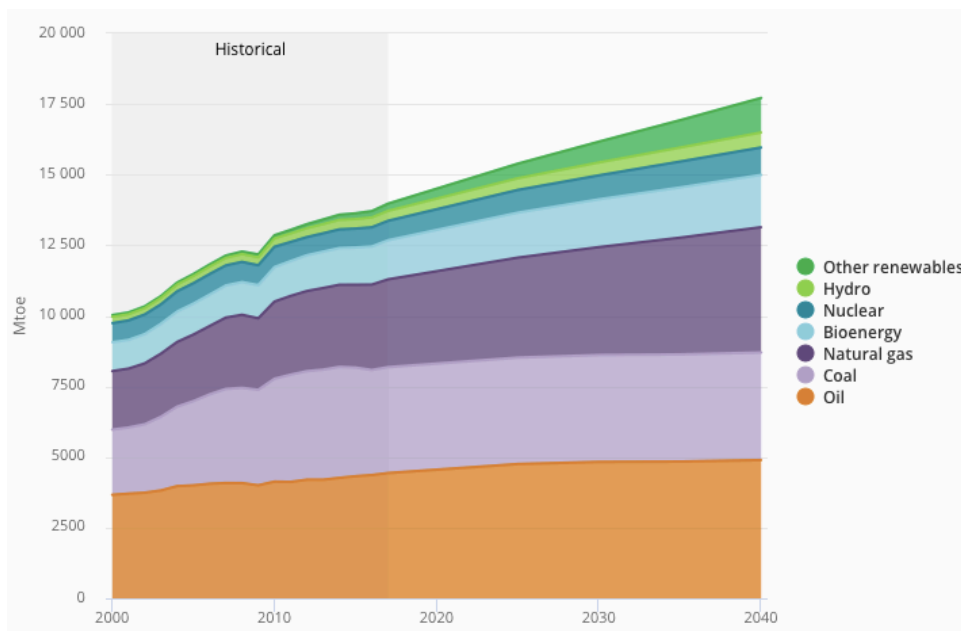
Figure 1.2: Global energy demand by source according the New Policies Scenario,
2000-2040 [3]

The graph predicts the energy demand from the oil and coal to be relatively constant, while a growing demand of energy originating from natural gas and renewables is predicted.

To end this subsection, we can conclude that the world population is expected to grow resulting in an increase of the global energy demand. Taking the global climate challenge in account, the growing energy must not be only supplied by the conventional fossil energy sources. Renewable energy systems will have to play a vital role in solving this problem which requires significant investment in these systems.

1.2. Renewable Energy Transition

As we have tried to show the importance of renewable energy systems in the previous subsection, let us take a look at the current and expected state of the renewable energy transition.

As stated before, in order to solve the global warming problem, governments are promoting the renewable energy transition process. The European Union, for example, has established the Renewable Energy Direction, which is responsible for overall policy for the production and promotion of renewable energy sources in EU. It requires the EU countries to produce at least 20% of its total energy needs and 10 % of its transport fuels from renewable sources by 2020 . A revised Renewable Energy Directive, proposed in 2016, sets a new target of 27% renewable sources for the total energy needs in 2030 [5].

However, the Renewable Energy Policy Network for the 21st Century (REN21), an international non-profit association, considers in its Renewables Global Status Report (GSR) the current transition to be more of an electricity transition than an energy transition [6]. This statement is supported by data provided by the International Renewable Energy Agency (IRENA), an intergovernmental organisation that supports countries in their transition to a sustainable energy future, and the International Energy Agency [7][8].

The International Energy Agency expects the fastest growth of renewables to be in the electricity sector, providing almost 30% of power demand in 2023 [8]. Currently, the renewable power sector is characterised by reducing costs, increased investment, record-setting installations and new, innovative business models that are creating rapid changes. In many parts of the world, renewable electricity is now less expensive than newly installed fossil and nuclear energy generation [6].

According to the IRENA, the total amount of electricity generated from renewables in 2016 was around 5886 TWh. The biggest portion of this number, 4049 TWh is generated by hydropower followed by 958 Twh accounted by the wind. Bio-energy, solar energy, geothermal energy and marine energy accounted respectively for 467 TWh, 329 TWh, 83 TWh and 1 TWh [7]. The pie-chart depicted in Figure 1.3 shows the corresponding percentages.
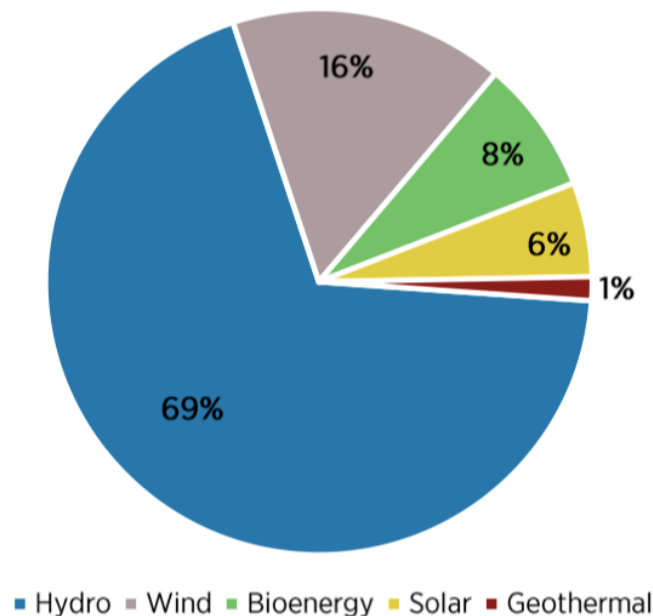
Figure 1.3: Renewable electricity production by energy source in 2016 [7]

The statement that the current transition is more of an electricity transition than an energy transition is also supported by the growth in the renewable electricity generation from 2015 tot 2016. The total renewable electricity generation in 2016 was increased by 6.7% compared to 2015 due rapid growth in solar and wind generation [7]. The numbers can be found in Figure 1.4.
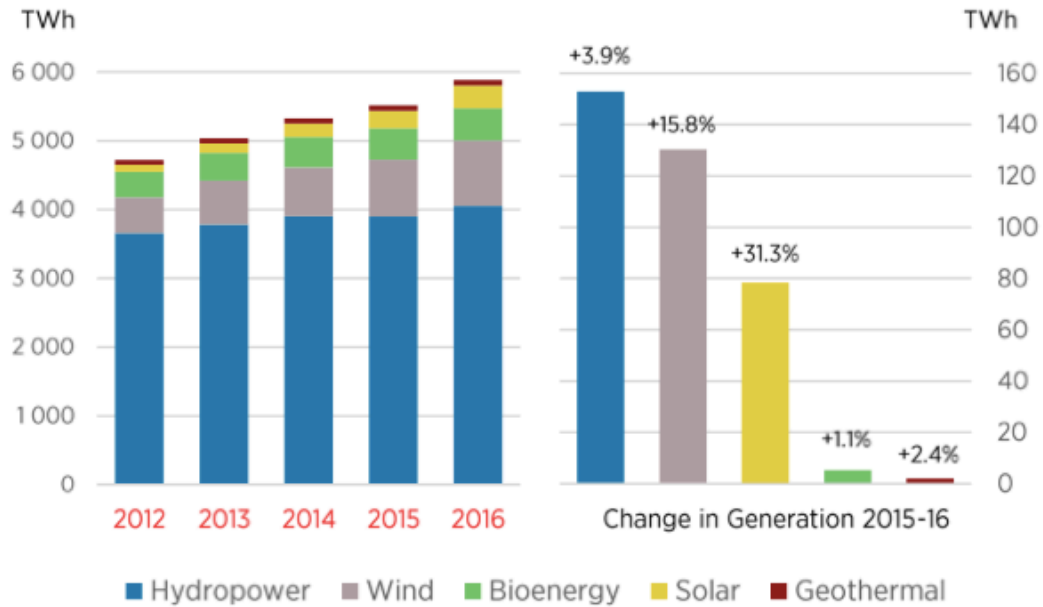
Figure 1.4: Growth in the renewable electricity generation [7]

The data from the IRENA provides us with two important insights regarding the marine energy in 2016: marine energy was a very small percentage of the total renewable electricity and the growth from 2015 to 2016 is even too small to be shown in the graph.

1.3. Ocean Energy

The offshore energy market is going through some significant changes due to several disruptive events, with the onshore shale oil revolution in the United States as the most impacting one [9]. The mentioned cost reduction of the renewable energy technologies, the up rise of electricity consumption by the energy end-users and the Chinese shift to cleaner energy mix, are also among the impacting disruptions regarding the offshore industry. Despite a relatively stable total production since 2000, the offshore natural gas production is increased by more than 50% and offshore electricity generation is increasing rapidly [9]. These events go together with the uprising of the offshore renewable technologies, harvesting electrical power from offshore wind and the ocean.

The ocean can be considered as an inexhaustible energy source and a significant resource for renewable electricity due to its size and predictability. However, ocean energy is currently one of the most unexploited energy source, contributing only 1.1 TWh (terawatt hour) to the total global energy production of 25,518 TWh in 2017 [10].

Ocean energy can be captured from tidal streams, ocean currents, ocean thermal energy conversion (OTEC), salinity gradients and wave power. The various technologies are at different stages of technical and commercial development, but it is expected that tidal and wave energy will provide the most significant contribution in the short term [11]. Recent studies and industry scenarios indicate that 337 GW of wave and tidal energy capacity could be harvested around the world by 2050. A third of this number, 100 GW, can be produced in Europe, providing 10 percent of Europe's electricity.[12].

The current status of the ocean energy industry can be illuminated by discussing the promising 398 MW MeyGen tidal stream project, located at an offshore site between the coast of Scotland and the island Of Stroma. Phase 1A of the project was completed in 2018, resulting in the largest tidal stream array in the world consisting of four 1.5MW turbines (6 MW rated capacity). The array has generated more than 12 GWh of energy up to date and the current 6 MW rated capacity is clearly a small portion of the 398 MW [13]. This tells us that the industry is making some significant steps, but still needs some time to really make an impact on the global energy mix.

Figure 1.5: Artistic impression of a tidal turbine deployed in the MeyGen project [14]

1.4. Wave Energy Converters

1.4.1. History

Wave power is the power obtained by harnessing the energy produced by the sea waves. Wave Energy Converters (WECs) are devices that are able to convert this wave energy into electrical power. First, wave energy is transformed into some form of mechanical energy which is then used to produce electricity and supply it to the grid by means of a generator. The global power potential of wave energy is estimated to be in the order of 10 TW [15].

WECs could play an essential role in fulfilling the electricity demand in remote islands as the access for electricity in such areas might be limited. This type of energy is environmentally friendly, available around the clock and can be installed in nearly every coastal area.
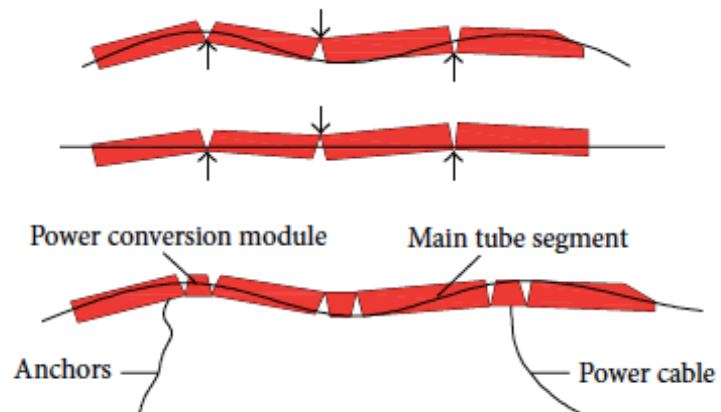
Figure 1.6: Working principle of the Pelamis [16]

The earliest patent to use energy from ocean waves was filed by Girard and his son in 1799 in Paris [17]. The first wave energy device studied in Europe was called 'the duck' and it was proposed in 1974 by Salter, who is considered as the founding father of wave energy [18]. The first wave energy converter that generated electricity into the grid was in 2004 by a device called the Pelamis [19], see Figure 1.6 . It is a device that consists of multiple interconnected floating devices operating parallel to the wave direction and basically riding the waves. Energy is harvested from the relative motion of the bodies with respect to the passing waves. The Pelamis has become one of the most studied WECs, but failed eventually because it was not capable to achieve the same levelized cost of energy as wind or solar energy [20].

After the Pelamis several other prototypes of Wave Energy Converters (WECs) have been shown to successfully produce electricity, but the efficiency of WECs compared to other energy converting devices is relatively low [18].

Delft University of Technology is developing a new wave energy converter concept called the Gyroscopic-Pendulum, which is the subject matter of this report.

1.4.2. WEC Types

Since there are many WEC concepts, the European Marine Energy Centre (EMEC) has identified eighth main types of WECs [21]:

(A) Attenuators

An attenuator is device that consists of multiple interconnected floating devices. It operates parallel to the wave direction and basically rides the waves. Energy is harvested from the relative motion of the bodies with respect to the passing waves. An example of an attenuator is the Pelamis.

(B) Point Absorbers
A point absorber is a floating device which is able to absorb wave energy from all directions due to its movement at or near the water surface. The device has small dimensions compared to the incident wave length and the motion of the top part relative to the base is converted into electrical power. Figure 1.7 gives an impression of a point absorber WEC.
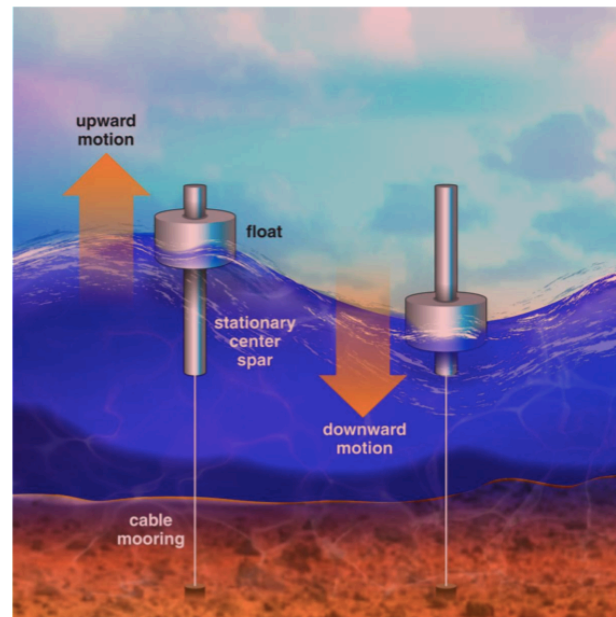
Figure 1.7: An illustration of a point absorber [22]

(C) Oscillating Wave Surge
Oscillating wave surge converters extract energy from wave surges and the movement of water particles within them. The arm oscillates as a pendulum mounted on a pivoted joint in response to the movement of water in the waves [19]. These devices are often designed in shallow waters due to the wave motions. AW-Energy is a company that has designed an OWS WEC called WaveRoller. AW-Energy has several WaveRoller projects currently under development or in the delivery phase.[23] Figure 1.8 gives an impression of the WaveRoller concept.

Figure 1.8: WaveRoller concept impression [23]

(D) Oscillating Water Column

An oscillating water column is an hollow structure that is partially submerged. The principle is based on enclosing a column of air on top of a column of water. Due to the motions of the waves, the water column will rise and fall causing compression or decompression of the air column. This air will flow through a turbine, causing it to rotate (in both directions) and generate electricity. The Università Mediterranea di Reggio Calabria has been developing an OWC concept called the REsonant Wave Energy Converter (REWEC3), which is incorporated into a vertical breakwater.[24] The REWEC concept can be seen in Figure 1.9
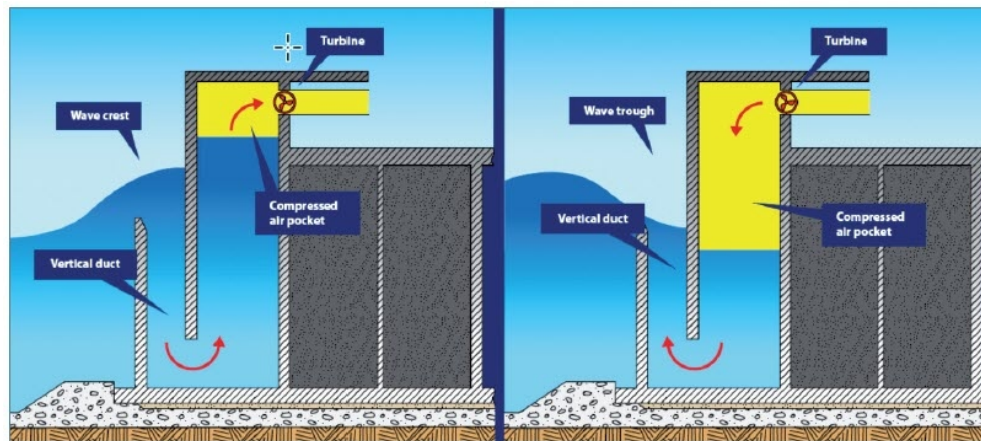
Figure 1.9: Scheme of REsonant Wave Energy Converter (REWEC) [24]

(E) Overtopping Devices

Overtopping devices capture sea water of incident waves in a storage reservoir above the sea level. The captured water will be released back to the sea, passing through turbines to generate power. An example of an overtopping device is the Wave Dragon, which is shown in Figure 1.10
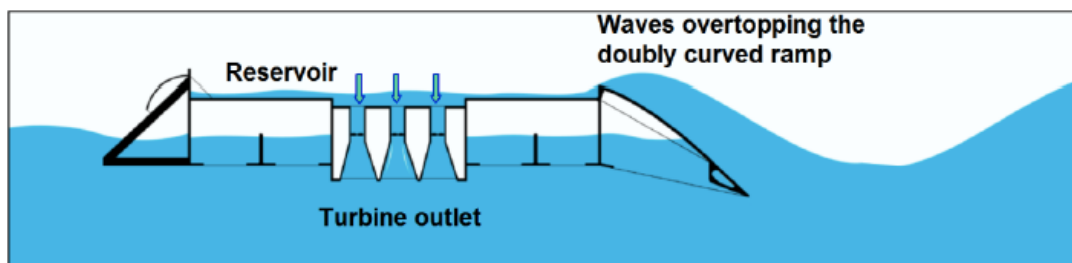
Figure 1.10: Working principle of the Wave Dragon [25]

(F) Submerged Pressure Differential

Submerged pressure differential WECs are submerged devices attached to the seabed. The sea level will rise and fall due to the motion of the waves. The change in sea level above the submerged device will induce a pressure differential resulting in vertical up and down motion of the device. These devices are often located near shore to take advantage of the wave phenomena, like shoaling and wave breaking, near to the shore. A well known example of this concept is the Archimedes Wave Swing, which is shown in Figure 1.11.
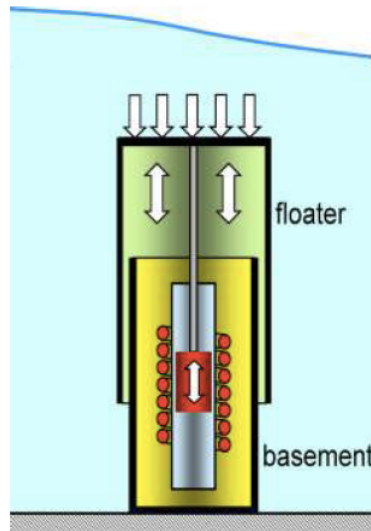
Figure 1.11: Working principle of the Archimedes Swing [26]

(G) Bulge Wave

Bulge wave technology consists of a moored rubber tube which is filled with water. The tube is heading into the waves. The water enters through the stern and the passing wave causes pressure variations along the length of the tube, creating a 'bulge'.[19] As the bulge travels through the tube it grows, gathering energy which can be used to drive a standard low-head turbine located at the bow, where the water then returns to the sea.[19] An example of bulge wave is the Anaconda wave energy converter, see Figure 1.12
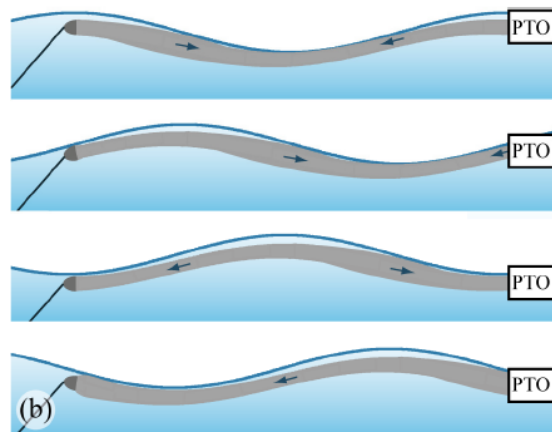
Figure 1.12: principle of bulge wave generation with direction of internal oscillatory flow and PTO [27]

(H) Rotating Mass

Rotating mass devices are concepts that make use of eccentric masses rotating about multiple axis or gyroscopes that cause precession. The devices consist of a surface floating buoy, with

the eccentric masses or gyroscopes inside it. The movement of the floater will cause for rotation of the masses, which can be converted into electrical power. Politecnico di Torino developed the Inertial Sea Wave Converter (ISWEC), a device that makes use of the gyroscopic effect to convert electricity from the pitch motion of the floater.[28] Figure 1.13 shows a concept drawing of the ISWEC.
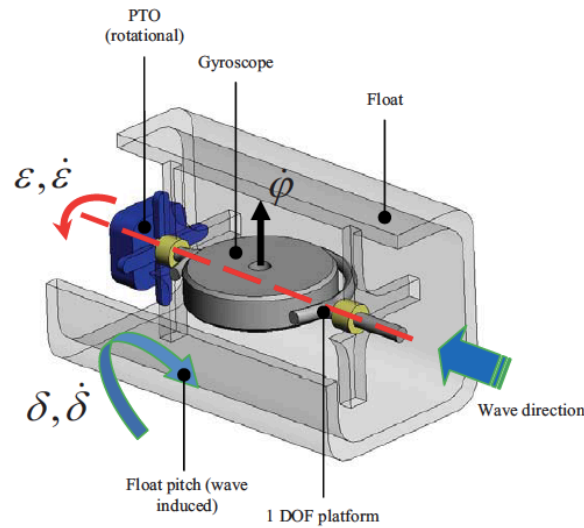
Figure 1.13: Concept drawing ISWEC [29]

Another interesting device is the PeWEC (Pendulum Wave Energy Converter), a device that allows to extract power by using the forces produced by a swinging pendulum enclosed into a sealed hull.[15]

1.4.3. Gyroscopic-Pendulum

Let us now introduce the new WEC concept called the gyroscopic-pendulum. This concept is a modification of the so called classical vertical axis pendulum, a type of point absorber device which is capable of producing mechanical power that is harvested from the rotation of the pendulum inside the floating module.

The new concept is proposed by adding a flywheel to create a gyroscopic effect with the aim to enhance the motions of the pendulum. The spinning disk and the torque originating from the weight of the pendulum, together create the gyroscopic effect, which drives the pendulum to rotate. This phenomenon is called precession. A preliminary concept drawing of the gyroscopic-pendulum is provided in Figure 1.14.
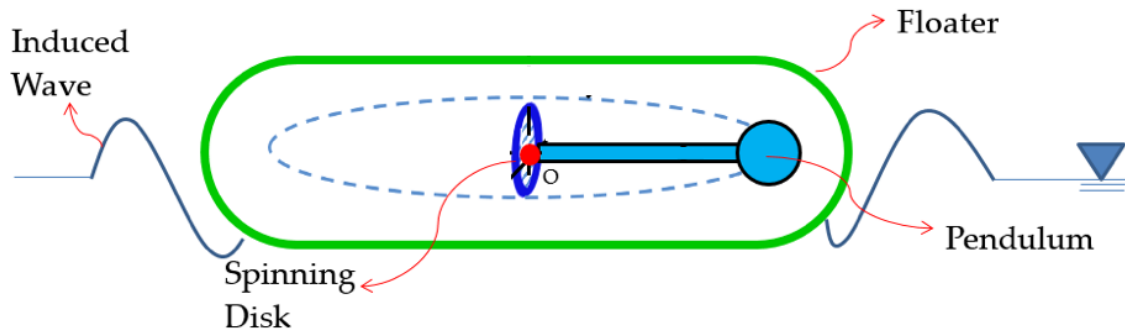
Figure 1.14: Concept drawing of the gyroscopic-pendulum WEC

The rotational motion of the pendulum, driven by the wave actions and the gyroscopic effect, will be converted in electrical power by using a Power-Take-Off (PTO) generator, which is placed in the same axis as the pendulum rotation.

In general, the main advantage of WEC concepts with no moving parts exposed to the sea environment is the intrinsic reliability of the device [15]. In case of the gyroscopic-pendulum, we can also consider the advantage of combining the controllable spinning disk with the rotating pendulum. This advantage comes from the ability to tune the pendulum rotation in order to reduce the losses associated to start-up and stopping as well as to provide control of its motions in different sea states [18].

1.4.4. Gyroscopic Precession

The gyroscopic effect used in our dynamical system has it's origins in the studies of Isaac Newton about the motions of the earth, which rotates around the sun while at the same time it also rotates around it's own axis [30]. However, it was Leonard Euler who proposed a mathematical model for this phenomenon and is also credited for [30].

The gyroscopic effect depends on the relationship between the angular momentum and external torque of a rotating system. Angular momentum $\vec{L}$ is a vector quantity that is proportional to the angular velocity of an rotating object. The definition is provided in Equation 1.1, in which I is the mass moment of inertia of the rotating body in kgm^2 and ω is rotational velocity of the object in rad/s.

$$\vec{L} = I\vec{\omega} \tag{1.1}$$

The law of conservation of angular momentum states that any change of angular momentum $\vec{L}$ in time can only occur if an external torque $\vec{G}$ is acting on the object.

$$\vec{G} = \frac{d\vec{L}}{dt} \tag{1.2}$$

From Equation 1.2 we can conclude that for rotating bodies a torque increases the angular momentum of the body in the direction of that torque. This is an analogy with the translating bodies, where an applied force $\vec{F}$ on the body increases the linear momentum $\vec{P}$ of the body in the direction of the applied force, see Equation 1.3.

$$\vec{F} = \frac{d\vec{P}}{dt} \tag{1.3}$$

Let us consider the following exemplary gyroscope modeled as the rigid body system shown in Figure 1.15.a. This particular gyroscope, often referred to as a gyro, is basically a rotor which is able to spin at a very high rate about its own axis. The mass of the rotor and it's mass moment of inertia are respectively denoted by m_r and $I_{r,x}$.
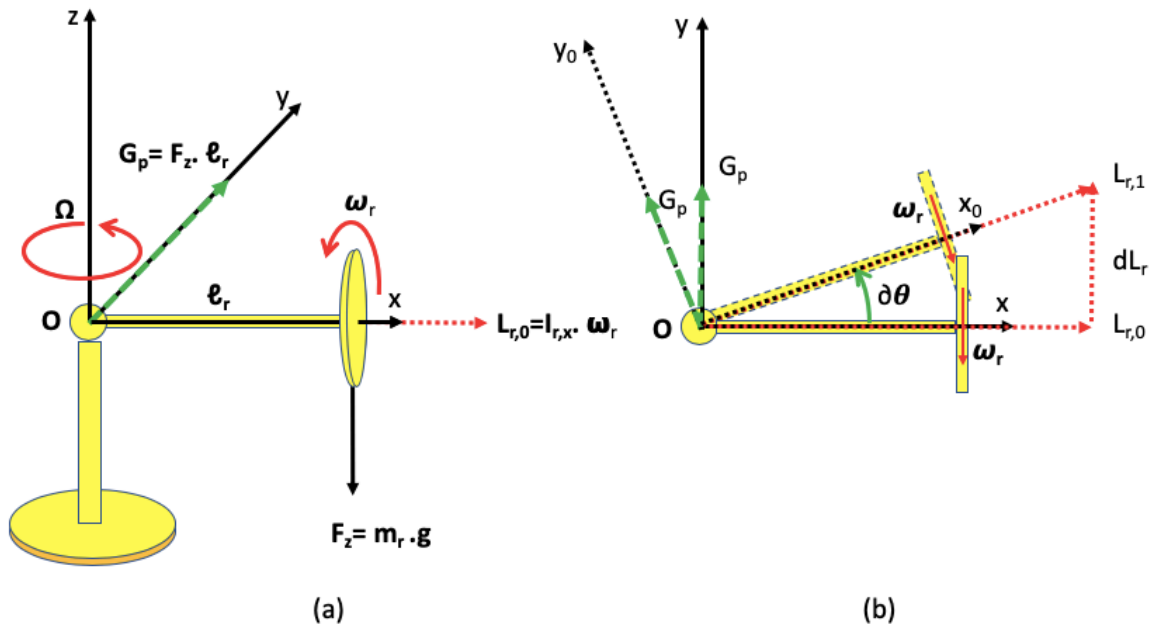
Figure 1.15: (a) Gyroscope system (b) Gyroscopic effect

The gyro is designed as such that the whole system is also able to rotate about the y and z axes. The rotation of the system about the z-axis is called "precession" and is denoted by Ω. The rate of spin of the rotor is much greater than the precessional velocity around the z-axis.

Without spinning the rotor about it's own axis, the system will rotate about the y-axis (fall downwards) due to gravity. However, if the rotor does spin, the gyroscopic effect will result in an angular velocity Ω of the system about the z-axis. This counter intuitive effect can be explained by the relationship between the angular momentum of rotor and the torque due to the mass of the rotor in distance l_r from the rotation point O of the system . The directions of the above mentioned angular momentum and torque are obtained by applying the so-called "right-hand rule".

We are interested in finding an expression for Ω in terms angular velocity of the rotor. Let us call a small rotation around the z-axis $\delta\theta$ and the small difference in angular momentum δL in the y-direction. The rate of spin of the rotor will be denoted by $\omega_{r,x}$. From Figure 1.15.b and our assumption that $\Omega << \omega_r$ we can see that the angular velocity about the z-axis is equal to the rate of change of the small rotation $\delta\theta$.

$$\Omega = \frac{\delta\theta}{dt} = \frac{1}{dt}\frac{d\vec{L}}{\vec{L}} = \frac{1}{\vec{L}}\frac{d\vec{L}}{dt} \tag{1.4}$$

Combining Equations 1.2 and 1.4 gives us the following relation:

$$\Omega = \frac{1}{\vec{L}}\vec{G} = \frac{m_r g l_r}{I_{r,x}\omega_r} \tag{1.5}$$

Equation 1.5 tells us that the angular velocity of the precessional motion equals the ratio of the torque divided by the angular momentum of the rotor. We can see that increasing the torque by increasing the mass and or the distance of the mass from the pivot point, will increase the precessional angular velocity. Also decreasing the angular momentum of the disk, by decreasing its mass moment of inertia and or angular velocity, will result in an higher precessional angular velocity.

1.5. Thesis Objectives

1.5.1. Research Question

This master of science thesis is centered about developing a mathematical model for a new type of wave energy converter, the gyroscopic-pendulum, and showing that this concept can improve the power efficiency compared to a classical vertical axis pendulum. The research can be divided into the following three parts:

- Create a mathematical model for the new concept

- Show the existence of the desired phenomenon, namely the increase of the average power efficiency due to the gyroscopic effect

- Explain the phenomenon

The final goal of the thesis is to provide an answer to the following research question:

In which ranges of amplitude and frequency of an imposed motion to the floater does the gyroscopic-pendulum result in an improved average power efficiency compared to a classical vertical axis pendulum?

In which the power efficiency is defined as the ratio between the average Power output of the system and the average power input to the system:

$$\eta = \frac{P_o}{P_i} \tag{1.6}$$

1.5.2. Approach

In order to achieve a successful closure of this research requires us to follow an approach that leads to a validated answer to the above research question, following tasks will have to be performed in the given order:

- Perform a literature study about the subject.

- Understand the necessary theories and assumptions that is required to model the system and derive the equations of motion.

- Validate the model by testing its response to certain inputs in the simulated conditions.

- Investigate different types of imposed motions to show within the reasonable movement of the vessel that the disk increases the power efficiency.

- Provide some kind of indication for what type of motions of the vessel, the presence of the disk improves the efficiency the most.

- Provide some explanation about the power efficiency resulting from the gyroscopic effect.

1.5.3. Thesis Outline
This thesis report is structured around five chapters in a certain way and order to make it relatively understandable despite the complexity of its subject.

- Chapter 1: Introduction starts with a global energy outlook followed by general information about the ocean energy and wave energy converters and the introduction of the Gyroscopic-Pendulum.

- In Chapter 2: Mathematical Model, the equations of motion are derived after introducing the model of the dynamical system along with the assumptions.

- In Chapter 3: Validation of the Model, the equations of the motion and the numerical model are validated by performing test under constant imposed motions of the floater.

- In Chapter 4: Hydrostatics, a preliminary shape of the floater will be introduced and the stability of the floating systems will be presented.

- In Chapter 5: Power Efficiency, the tests are explained and the results obtained from numerical simulations are presented.

- In Chapter 6: Conclusion and Recommendations, the conclusions and recommendations based on the results obtained from the numerical simulations are presented.

2

Mathematical Model

2.1. Introduction

In order to understand, explain and predict the behaviour of our device, we need to first formulate a mathematical model of it. This will be the subject matter of this chapter.

We will start with describing our model accompanied by assumptions regarding the device and interactions between its components in order to formulate the model. Some necessary theoretical concepts will be reviewed and at the end of the chapter we will display the derivation of the equations of motion for our dynamical system.

2.2. Gyroscopic-Pendulum Model

The gyroscopic-pendulum consists of a rotating disk connected to a rotating vertical axis pendulum which is attached to a floater. The motions of the floater impose certain motions to the pendulum, which can be enhanced by the rotating disk due to the gyroscopic effect. The gyroscopic-pendulum is an 8-DOF system, of which 6-DOF are accounted by the floater, 1-DOF is accounted by the rotating pendulum around the vertical axis and 1-DOF is accounted by the rotation of the disk around the pendulum axis. A preliminary concept drawing of the system is provided in Figure 2.1.
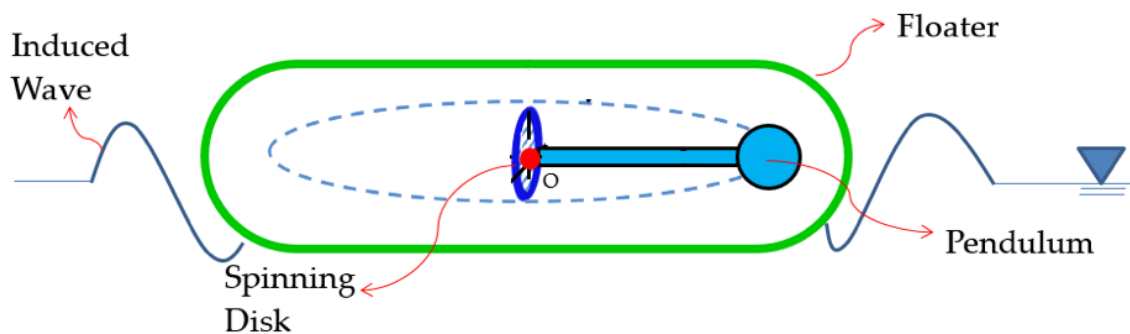
Figure 2.1: Concept drawing of the gyroscopic-pendulum WEC

In this study we will simplify the dynamical system by excluding the surge, sway and heave motions of the floater. The yaw motion of the floater is decoupled from the pendulum motion, because the generator will be installed in the pendulum axis of rotation, hence we also neglect the yaw motion of the floater. The motions of the pendulum are coupled with the remaining roll and pitch motions of the floater. These assumptions result in the dynamical system consisting of the following four degrees of freedom:

- Disk rotation $\phi_d(t)$, rotation about the pendulum axis

- Floater pitch motion $\theta_f(t)$, rotation about the earth-fixed Y-axis

- Floater roll motion $\phi_f(t)$, rotation about the earth-fixed X-axis

- Pendulum yaw motion $\psi_p(t)$, rotation about the body-fixed z-axis attached to the floater

Two right-handed Cartesian coordinate systems will be used to describe the motions of this system: an earth-fixed inertial coordinate system denoted by *XYZ* and a body-fixed coordinate system attached to the floater denoted by *xyz*. The motions in the body-fixed coordinate system are relative to earth-fixed coordinate system. Figure 2.2.a shows the coordinate systems.
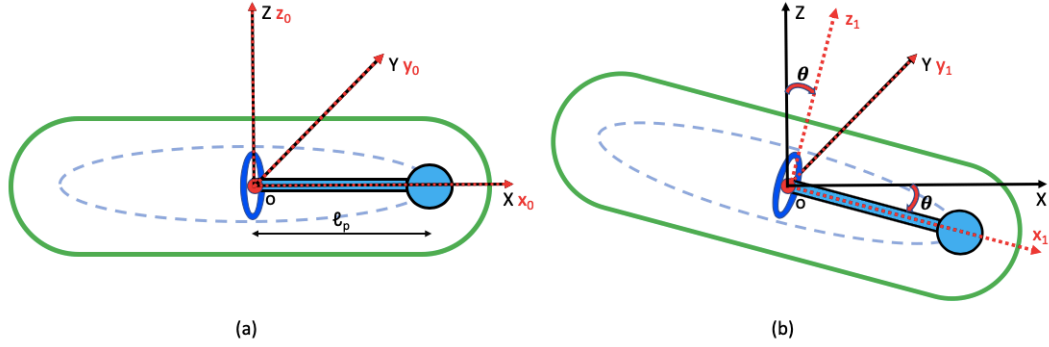
Figure 2.2: a). GP configuration and coordinate system b). Rotation example

Let us assume that the pendulum is a point mass located at l_p from the center of rotation *O* which is at the origin of the body-fixed coordinate system. The rotation of the pendulum around the body-fixed coordinate z_0-axis is denoted by ψ_p and the rotation of the disk around the pendulum axis is denoted by ϕ_d. The floater is assumed to have its COG and rotation point at the same point and is also rotating around point *O*. The roll ($\phi_f(t)$) and pitch ($\theta_f(t)$) motions of the floater are respectively rotation around the earth-fixed *X-axis* and *Y-axis*.

All the components are described as a rigid body, which means the distance between two points in a body remains unchanged as it moves. Figure 2.2.b shows a exemplary positive pitch motion of the floater to provide some understanding of the pendulum rotation.

2.3. Lagrangian Formalism

There are two well known methods that can be used to derive the equations of motion of mechanical systems; the Newton-Euler method and the Euler-Lagrange method.

Newton-Euler method is based on Newtonian mechanics, which deals with vector quantities such as force and momentum, while the Euler-Lagrange method is based on Lagrangian mechanics, which deals with scalar energy components. Use of Newtonian mechanics becomes complex compared to the Lagrangian mechanics when we have to deal with multi-body systems with constraints [31], because "Newton's equations treats each rigid body separately and explicitly model the constraints through the forces required to enforce them, while Lagrange and d'Alembert provided systematic procedures for eliminating the constraints from the dynamic equations, typically yielding a simpler system of equations" [18].

Since we are considering a 4-DOF multi-body system with rigid body constraint, we will use the Euler-Lagrange method to derive the equations of motion of our system. The Euler-Lagrange method is based on a systematic approach which is known as the "Lagrangian Formalism". The equations of motions are derived by solving the differential equation that is called the "Euler-Lagrange Equation", which can be found in Equation 2.1.

$$\frac{d}{dt}\frac{\partial \mathcal{L}}{\partial \dot{q}_i} - \frac{\partial \mathcal{L}}{\partial q_i} = Q_i \qquad (2.1)$$

This equation is applicable to any N-DOF system in which q_i are the generalized coordinates, Q_i are the generalized forces and $\mathcal{L}(q_i, \dot{q}_i, t)$ is the so called "Lagrangian". The Euler-Lagrange equations states that the time derivative of the derivative of the Lagrangian with respect to the velocity of the system minus the derivative of the Lagrangian with respect to the displacement is equal to the generalized force.

$$\mathcal{L} = \mathcal{T} - \mathcal{V} \qquad (2.2)$$

Since $\mathcal{T}$ and $\mathcal{V}$ are representations of the kinetic and potential energy respectively, hence the Euler-Lagrange equation contains scalar quantities. The kinetic energy is proportional to the square of the translational or angular velocities of the components and the potential energy can be obtained from the position of the components in a gravitational field (gravitational potential energy).

$$\mathcal{T}_{t,i} = \frac{1}{2}m_i v_i^2 \qquad (2.3)$$

$$\mathcal{T}_{r,i} = \frac{1}{2}I_i \omega_i^2 \qquad (2.4)$$

$$\mathcal{V}_i = m_i g h_i \qquad (2.5)$$

$\mathcal{T}_{t,i}$ and $\mathcal{T}_{r,i}$ are respectively the translational kinetic energy and rotational kinetic energy of component i. m_i is the mass of component i in [kg], v_i is the velocity of component i in [m/s], I_i is the moment of inertia of component i in $[kgm^2]$ and ω_i is the angular velocity of component i in [rad/s]. The gravitational acceleration in $[m/s^2]$ is denoted by g and h_i is the position of component i in the Z-axis.

2.4. Derivation of Equations of Motion

2.4.1. Mass Moment of Inertia

Since all motions of the system are rotational motions, we need to introduce an important quantity that dominate these type of motions. While translational motions are governed by the equation of the form $F = m\,a$, the rotational motions are governed by the equation of the form $T = I\alpha$, in which $I\ (kg/m^2)$ is called the "mass moment of inertia". It is a measure of resistance to an angular acceleration due to an applied torque, while the mass is a measure of resistance to an linear acceleration due to an applied force. The mass moment of inertia depends on the distribution of mass of a body and the axis of rotation.

Let us derive the general equation form of the mass moment of inertia for an arbitrary object by considering a general shape of body with total mass M shown in Figure 2.3.
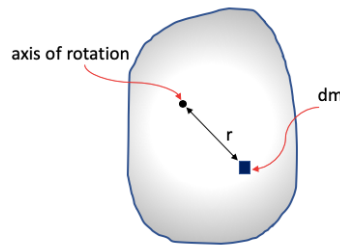
Figure 2.3: General shape with total mas M

For the mass of an infinitesimal small part of the body dm with a distance r from the axis of rotation, the mass moment of inertia is given by the following equation:

$$dI = r^2 dm \tag{2.6}$$

If we take the sum over all of the mass elements, we end up with the general formula for the mass moment of inertia.

$$I = \int dI = \int_0^M r^2 dm \tag{2.7}$$

Figure 2.4 gives an overview of the mass moment of inertia of a few common shapes.
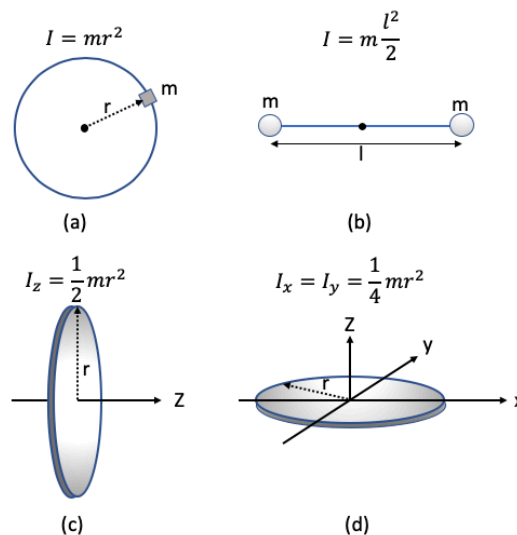
Figure 2.4: (a) Point mass around axis perpendicular to the paper, (b) Two point masses around axis perpendicular to the paper, (c) Disk around z-axis, (d) Disk around x and y-axis

2.4.2. Linear Velocity of the Pendulum

Coordinate Transformation

In order to compute the kinetic and potential energy of the pendulum, it is convenient to find its position and linear velocity relative to the earth-fixed coordinate system. This can be found by using the so called Euler angles to decompose the body-fixed position vector in the earth-fixed coordinate system. The Euler angles are the three principal angles, roll (ϕ), pitch (θ) and yaw (ψ), introduced by Leonard Euler to describe the orientation of a rigid body or a reference frame with respect to a fixed coordinate system.[32]

We can apply rotations of the Euler angles by means of rotation matrices.

$$\mathbf{R}_{\phi x} = \begin{vmatrix} 1 & 0 & 0 \\ 0 & c\phi_f & s\phi_f \\ 0 & -s\phi_f & c\phi_f \end{vmatrix}, \mathbf{R}_{\theta y} = \begin{vmatrix} c\theta_f & 0 & s\theta_f \\ 0 & 1 & 0 \\ -s\theta_f & 0 & c\theta_f \end{vmatrix}, \mathbf{R}_{\psi z} = \begin{vmatrix} c\psi_f & s\psi_f & 0 \\ -s\psi_f & c\psi_f & 0 \\ 0 & 0 & 1 \end{vmatrix} \tag{2.8}$$

The rotation matrix $\mathbf{R_{ij}}$ is describing a rotation angle i about the *j-axis* (according to our positive axis directions), in which the s·=sin(·), and c ·=cos(.).

A coordinate transformation matrix can be used to describe an object in a rotated coordinate system, while keeping the object itself fixed. It is closely related to the rotation matrices and has the following important property.[32]

$$\mathbf{R_e^b}(\phi, \theta, \psi) = \mathbf{R_b^e}(\phi, \theta, \psi)^T \tag{2.9}$$

In which $\mathbf{R_e^b}$ is the orthogonal coordinate transformation matrix and the subscript e and superscript b respectively stand for 'from' and 'to' a coordinate system. In this case $\mathbf{R_e^b}$ is representing a transformation matrix which can transform a vector from the earth-fixed coordinate system to the body-fixed coordinate system.

An important concept in rotational motions is the notion of order of rotation, since it affects the position and orientation of an object. In general there are many rotation orders possible and once again we make a simplification by choosing one for our computation of the pendulum position and its velocity:

Pendulum Rotation (ψ_p) - Floater Pitch(θ_f) - Floater Roll (ϕ_f)

The rotation matrices given in Equation 2.8 also correspond to our defined system angles (ϕ_f, θ_f, ψ_p) and with the chosen rotation order we can compute our desired transformation matrix.

$$\mathbf{R_b^e}(\phi_f, \theta_f, \psi_p) = \mathbf{R_e^b}(\phi_f, \theta_f, \psi_p)^T = (\mathbf{R}_{\psi z}.\mathbf{R}_{\theta y}.\mathbf{R}_{\phi x})^T \tag{2.10}$$

Position and Velocity Vectors

The pendulum is assumed to be a point mass with a distance l_p from the origin of the earth-fixed coordinate system and its initial position in the proposed configuration is given by the following vector in the body-fixed coordinate system:

$$\vec{p}_{(0)}^b = \begin{vmatrix} l_p \\ 0 \\ 0 \end{vmatrix} \tag{2.11}$$

The position of the pendulum in time, in the earth-fixed coordinate system, can be now found by the following transformation.

$$\vec{p}^e(t) = \mathbf{R_b^e}(\psi_p, \theta_f, \phi_f)\vec{p}_{(0)}^b \tag{2.12}$$

Taking the time derivative of the $\vec{p}^e(t)$ vector results in the linear velocity vector $\vec{v}^e(t)$.

2.4.3. Angular Velocities of the Disk

Finding the angular velocities of the disk is necessary for the computation of the kinetic energy of it. The disk is free to rotate around the pendulum axis in its own COG. Moreover, the disk is also subjected to the rotational motions imposed by the pitch and roll motions of the floater and the pendulum rotation. However, in contrary to the pendulum, we cannot model the disk as a point mass, since we are interested in the rotations of the disk in its own COG. Instead we try to express its angular velocities relative to the earth-fixed coordinate system directly by means of transformations.

Let us start by stating that rotation matrices are in fact orthogonal matrices, which have the property stated in Equation 2.13.

$$\mathbf{R}^T\mathbf{R} = \mathbf{I}$$
$$\mathbf{R}\mathbf{R}^T = \mathbf{I} \tag{2.13}$$

If we take the derivatives of both expressions in time we end up with the following two equations.

$$\dot{\mathbf{R}}^T\mathbf{R} + \mathbf{R}^T\dot{\mathbf{R}} = \mathbf{0}$$
$$\mathbf{R}\dot{\mathbf{R}}^T + \dot{\mathbf{R}}\mathbf{R}^T = \mathbf{0} \tag{2.14}$$

In which $\mathbf{R}^T\dot{\mathbf{R}}$ and $\dot{\mathbf{R}}\mathbf{R}^T$ are skew matrices, implying that the off-diagonal elements satisfy $ij = -j$ for i ≠ j, while the diagonal elements are zero.[32]

Let us now try to derive the angular velocities of a general system in the earth-fixed and body-fixed coordinate systems by starting off with the Equation 2.12 for a general vector q and its derivative in time.

$$\vec{q}(t) = \mathbf{R_b^e}\vec{p}$$
$$\dot{\vec{q}}(t) = \dot{\mathbf{R_b^e}}\vec{p} \tag{2.15}$$

In which $q(t)$ is the changing coordinate of p while p is the constant coordinate in the body-fixed frame and $\dot{q}(t)$ is the linear velocity v_e of p in the earth-fixed coordinate frame.

A pre-multiplication of both sides of the expression for $\dot{q}(t)$ with $\mathbf{R}^T$ results in the following equation.

$$\mathbf{R_b^e}^T\dot{\vec{q}}(t) = \mathbf{R_b^e}^T\dot{\mathbf{R_b^e}}\vec{p} \tag{2.16}$$

The left hand side of Equation 2.16 is representing the linear velocity v_b in the body-fixed frame, while $\mathbf{R_b^e}^T\dot{\mathbf{R_b^e}}$ encodes the angular velocity in the body-fixed frame ω_b. This can be expected to be true, since it is known that $v = \omega r$.

Let us also combine the two expressions in Equation 2.15 resulting into a new expression for the linear velocity in the earth-fixed coordinate system $\dot{\vec{q}}(t)$.

$$\dot{\vec{q}}(t) = \dot{\mathbf{R_b^e}}\mathbf{R_b^e}^T\vec{q}(t) \tag{2.17}$$

The $\dot{\mathbf{R_b^e}}\mathbf{R_b^e}^T$ encodes the angular velocity in the earth-fixed coordinate system ω_e.

Let us compute the above matrix multiplication ($\dot{\mathbf{R_b^e}}\mathbf{R_b^e}^T$) to find the angular velocities of the disk in the earth-fixed coordinate system. This can be computed by substituting the rotation matrices of our system according to our chosen order of rotation, taking the orthogonality property of the rotation matrices in consideration and correctly using the product rule.

$$
\begin{aligned}
\dot{\mathbf{R}}_{\mathbf{b}}^{\mathbf{e}}\mathbf{R}_{\mathbf{b}}^{\mathbf{e}T} &= \frac{d}{dt}(\mathbf{R}_{\phi_{dx}}\mathbf{R}_{\psi_z}\mathbf{R}_{\theta y}\mathbf{R}_{\phi x})(\mathbf{R}_{\phi_{dx}}\mathbf{R}_{\psi_z}\mathbf{R}_{\theta y}\mathbf{R}_{\phi x})^T \\
&= (\dot{\mathbf{R}}_{\phi_{dx}}(\mathbf{R}_{\psi_z}\mathbf{R}_{\theta y}\mathbf{R}_{\phi x}) + \mathbf{R}_{\phi_{dx}}(\dot{\mathbf{R}}_{\psi_z}\mathbf{R}_{\theta y}\mathbf{R}_{\phi x} + \mathbf{R}_{\psi_z}(\dot{\mathbf{R}}_{\theta y}\mathbf{R}_{\phi x} + \mathbf{R}_{\theta y}\dot{\mathbf{R}}_{\phi x})))\mathbf{R}_{\phi x}^T\mathbf{R}_{\theta y}^T\mathbf{R}_{\psi_z}^T\mathbf{R}_{\phi_{dx}}^T \\
&= \dot{\mathbf{R}}_{\phi_{dx}}\mathbf{R}_{\phi_{dx}}^T + \mathbf{R}_{\phi_{dx}}\dot{\mathbf{R}}_{\psi_z}\mathbf{R}_{\psi_z}^T\mathbf{R}_{\phi_{dx}}^T + \mathbf{R}_{\phi_{dx}}\mathbf{R}_{\psi_z}\dot{\mathbf{R}}_{\theta y}\mathbf{R}_{\theta y}^T\mathbf{R}_{\psi_z}^T\mathbf{R}_{\phi_{dx}}^T + \mathbf{R}_{\phi_{dx}}\mathbf{R}_{\psi_z}\mathbf{R}_{\theta y}\dot{\mathbf{R}}_{\phi x}\mathbf{R}_{\phi x}^T\mathbf{R}_{\theta y}^T\mathbf{R}_{\psi_z}^T\mathbf{R}_{\phi_{dx}}^T
\end{aligned}
\tag{2.18}
$$

Equation 2.18 results in a skew 3x3 matrix of the following form:

$$
\mathbf{C} = \begin{vmatrix} 0 & -\omega_z & \omega_y \\ \omega_z & 0 & -\omega_x \\ -\omega_y & \omega_x & 0 \end{vmatrix}
\tag{2.19}
$$

It turns out that the non-zero entries in matrix C are the angular velocities of the system, and in our case that of the disk in the earth-fixed coordinate system.[32]

We are now able to construct the vector $\vec{\omega}_d = [\omega_x; \omega_y; \omega_z]^T$ resulting in the following:

$$
\vec{\omega}_d = \begin{vmatrix} \dot{\phi}_d + sin(\psi_p)\dot{\theta}_f + cos(\psi_p)cos(\theta_f)\dot{\phi}_f \\ sin(\phi_d)\dot{\psi}_p + cos(\phi_d)cos(\psi_p)\dot{\theta}_f - cos(\phi_d)sin(\psi_p)cos(\theta_f)\dot{\phi}_f + sin(\phi_d)sin(\theta_f)\dot{\phi}_f \\ cos(\phi_d)\dot{\psi}_p - sin(\phi_d)cos(\psi_p)\dot{\theta}_f + sin(\phi_d)sin(\psi_p)cos(\theta_f)\dot{\phi}_f + cos(\phi_d)sin(\theta_f)\dot{\phi}_f \end{vmatrix}
\tag{2.20}
$$

This vector is then used to compute the kinetic energy of the disk. The expression for the kinetic energy of the disk can be verified by considering the position of a point with a distance d from the COG of the disk and finding it's linear velocity. The kinetic energy of the whole disk can be found by taking the following integral:

$$
K_d = \frac{1}{2}\frac{m_d}{\pi r_d^2}\int_0^{2\pi}\int_0^{r_d}(\dot{x}_d^2 + \dot{y}_d^2 + \dot{z}_d^2).r.dr.d\phi_d
\tag{2.21}
$$

2.4.4. Energy of the System
Kinetic Energy
The motions of the pendulum and of the disk result in the kinetic energy in our system. Let us first consider the kinetic energy of the pendulum (assumed to be a point mass). It can simply be found by using the known equation for kinetic energy of a translating body.

$$
\mathcal{T}_p = \frac{1}{2}m_p\vec{v_p}(t)^2
\tag{2.22}
$$

In which m_p is the mass of the pendulum and $v_p(t)$ is its velocity in time. The velocity of the pendulum can be found by taking the derivative of its position in time.

$$
\vec{v_p}(t) = \frac{d\vec{p_p}(t)}{dt}
\tag{2.23}
$$

The kinetic energy of the disk cannot be computed in the simple manner used for the pendulum due to the coupled angular velocity terms of the disk. The rotational form of the kinetic energy of the disk in direction i can be computed according to the following equation:

$$
\mathcal{T}_{d,i} = \frac{1}{2}I_{d,i}\omega_{d,i}^2
\tag{2.24}
$$

The total kinetic energy of the system is computed by simply adding up the kinetic energy of the pendulum and of the disk.

$$
\mathcal{T}_{total} = \mathcal{T}_p + \mathcal{T}_{d,total}
\tag{2.25}
$$

Potential Energy

The pendulum and the disk contain gravitational potential energy that is proportional to the position of the pendulum and the disk in the Z-axis. It can be computed by first finding the position vector of the center of mass of the pendulum-disk combination. let us first find the position of the center of mass of the pendulum+disk:

$$l_{tot} = \frac{m_p l_p}{m_p + m_d} \tag{2.26}$$

The position of the combined mass in the *z-direction* can be now found by multiplying the third element (*z-direction*) of the position vector of the pendulum with the l_{tot}:

$$h(t) = l_{tot}\vec{p}^e(1,3) \tag{2.27}$$

The potential energy of the system can be computed according to the following equation:

$$\mathcal{V}_{total} = (m_p + m_d)gh(t) \tag{2.28}$$

2.4.5. Euler-Lagrange Equation

Since we have found the kinetic and potential energies of the system, we can perform the necessary substitutions to compute the Lagrangian and eventually solve the Euler-Lagrange Function.

Let us start with computing the Lagrangian $\mathcal{L}$ for our dynamical system.

$$\mathcal{L} = \mathcal{T} - \mathcal{V} = \mathcal{T}_{total} - \mathcal{V}_{total} \tag{2.29}$$

In our model we do not consider any external forces, meaning we have to solve the following form of the Euler-Lagrange Function:

$$\frac{d}{dt}\frac{\partial \mathcal{L}}{\partial \dot{q}_i} - \frac{\partial \mathcal{L}}{\partial q_i} = 0 \tag{2.30}$$

We substitute each degree of freedom ($\psi_p, \phi_f, \theta_f, \phi_d$) in the generalized coordinate q_i and solve the above differential equation. This will result in four equations of motion (one equation for each degree of freedom), which can be found in the appendix.

3

Validation of the Model

3.1. Introduction

In Chapter 2: Mathematical Model, we have presented the derivation of the equations of motion for our dynamical system. The focus of this chapter is the validation of the equations of motions by means of a numerical model.

We will start with introducing our numerical model followed by the validation of the equations of motions. The validation focuses on the correctness of the order of rotation and the rotations of the components with respect to the correct coordinate systems. very simple, yet powerful, tests are performed under constant imposed motions of the floater.

3.2. Numerical Model

3.2.1. System Dimensions

The numerical model consists of two systems, the 4-DOF gyroscopic-pendulum (gp) and the 3-DOF classical pendulum (cp). The equations of motion for the cp can be derived from the equations of motion of the gp by getting rid of the disk (in terms of mass, mass moment of inertia and degree of freedom). Since we are imposing both pitch and roll motions, we do not need to consider the shape, dimensions and thus hydrodynamics of the floater for both systems. We will also neglect the damping terms for the disk and the pendulum, since we are only interested in their rotations in the correct coordinate system. Let us start with presenting the constants and system dimensions that are used in our numerical model:

- Mass of the pendulum m_p = 30 kg
- Length of the pendulum l_p = 1 m
- Mass of the disk m_d = 20 kg
- Radius of the disk r_d = 0.25 m
- Gravity of earth g = 9.81 m/s^2

Performing a dimension analysis is not part of this thesis, hence dimensions for our model are just some chosen numbers that are thought to be realistic.

3.2.2. ODE Solver

Dynamic systems are represented by ordinary differential equations due to their property that how a system is changing in time is a function of its current state. Our equations of motions are second order non-linear ordinary differential equations, making it very difficult (impossible) to find analytical solutions for them. Therefore, the numerical model is designed to find numerical solutions to these differential equations.

The most important function used in the numerical model is the so called Ordinary Differential Equation solver. The term 'ordinary' refers to a differential equation which contains

functions of only one independent variable, for example time. Its counterpart is the term 'partial' which refers to differential equations which can be with respect to more than one independent variables e.g. time and space.

We will make use of the ODEINT function in python. Numerical ODE solvers can only work with first order differential equations, so we need to transforms the high order, in our case second order, differential equations into a set of first order differential equations. This transformation can be constructed by use of a concept called the 'state space representation'. We can explain the method by considering the example of a damped mass-spring system of which the linearized equation of motion is given in Equation 3.1.

$$m\ddot{x}(t) = -b\dot{x}(t) - kx(t) + f(t) \tag{3.1}$$

The set space representation requires us to introduce new variables in the following manner:

$$
\begin{aligned}
x(t) &= x_1 \\
\dot{x}(t) &= x_2 \\
f(t) &= f_1
\end{aligned}
\tag{3.2}
$$

Substituting the new variables in Equation 3.1 gives us the the following two first order differential equations:

$$
\begin{aligned}
\dot{x}_1 &= x_2 \\
\dot{x}_2 &= -\frac{b}{m}x_2 - \frac{k}{m}x_1 + \frac{1}{m}f_1
\end{aligned}
\tag{3.3}
$$

We can rewrite these equations in a matrix form of $\dot{X} = \mathbf{A}X + \mathbf{B}F$.

$$
\begin{vmatrix} \dot{x}_1 \\ \dot{x}_2 \end{vmatrix} = \begin{vmatrix} 0 & 1 \\ \frac{-k}{m} & \frac{-b}{m} \end{vmatrix} \cdot \begin{vmatrix} x_1 \\ x_2 \end{vmatrix} + \begin{vmatrix} 0 \\ \frac{1}{m} \end{vmatrix} \cdot |f_1|
\tag{3.4}
$$

These matrices will be the inputs for the ode solver which will gives us the outputs in terms of rotations and angular velocities of the systems.

3.3. Validation

3.3.1. Imposed Positive Pitch Motion

Let us now perform our first test in which we give a positive rotation to the pendulum of $\psi_p = \frac{\pi}{2}$ rad and then impose a constant pitch motion of $\theta_f = \frac{\pi}{2}$ rad and a constant roll motion of $\phi_f = 0$ rad, see Figure 3.1.a. The rotations of the floater are around the earth-fixed axis and according to our chosen rotation order (first pitch and then roll).

Figure 3.1.b shows an (unit) circle with the position of the pendulum in the body-fixed coordinate system after the imposed motions. The i in x_i, y_i, z_i stands for the number of rotation, e.g. x_1, y_1, z_1 correspond to the body-fixed coordinates of the first imposed motion (roll). The body-fixed $z_i - axis$ always points outward of the paper and the positive rotation of the pendulum is depicted according to the right-hand rule. This also tells us where the zero rotation should be depicted in the circle. The expected rotation of the pendulum is shown in red.
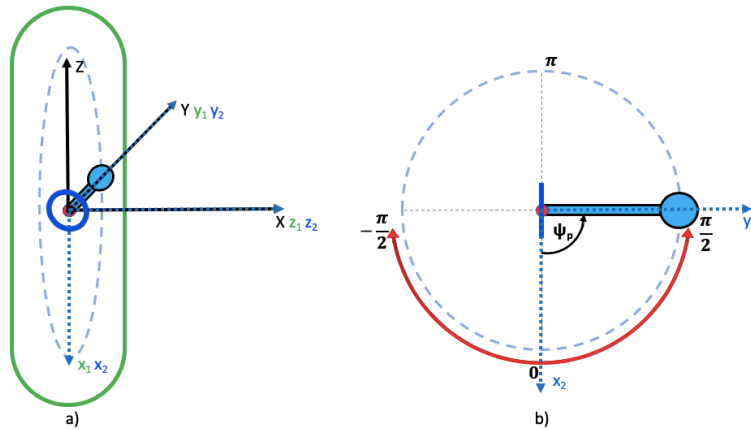
Figure 3.1: a). Orientation of the system after performing the imposed motions b). Expected rotation of the pendulum

In this case, the pendulum is positioned at $\frac{\pi}{2}$, hence we expect it to perform an undamped rotation about the $z_2 - axis$ starting from $\frac{\pi}{2}$ to $-\frac{\pi}{2}$, see Figure 3.1.b. Since we do not introduce damping in our system, the energy must be conserved.

From Figure 3.2, we can see that the results obtained form the numerical model is in agreement with our expectation.
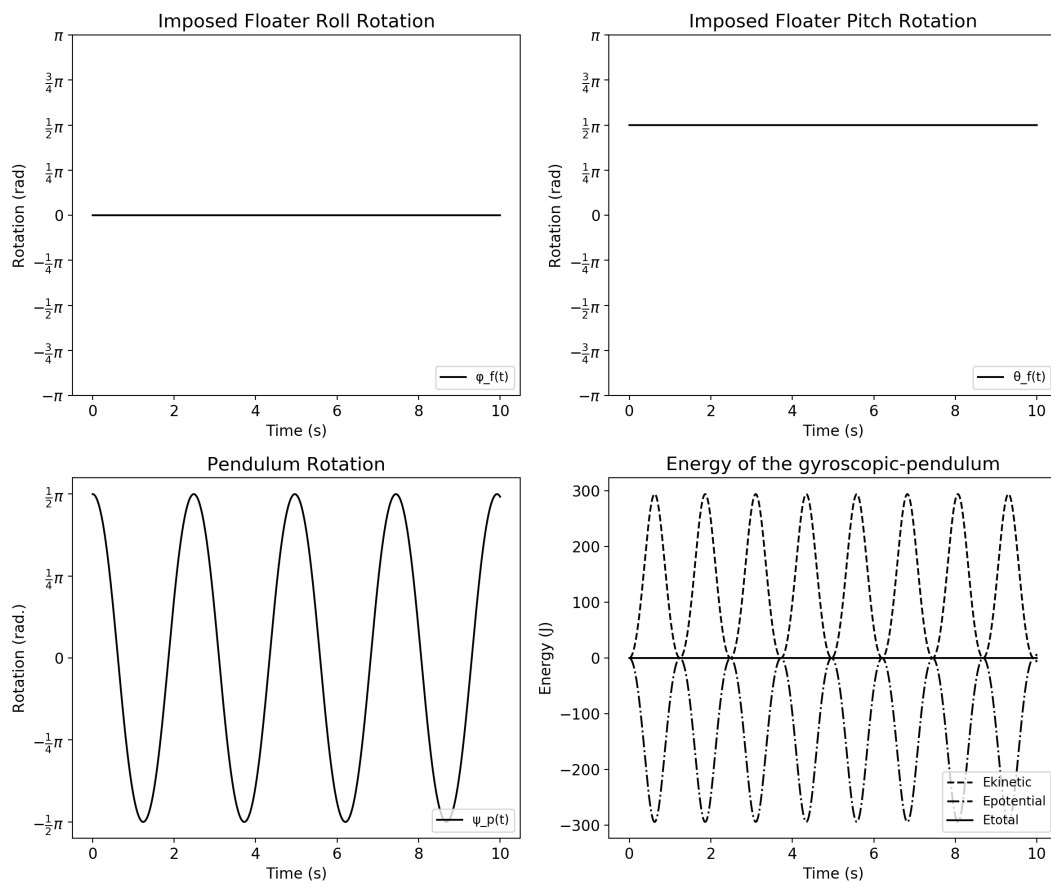
Figure 3.2: Results obtained from the numerical model

3.3.2. Imposed Positive Roll Motion

The second test consists of imposing a constant pitch motion of $\theta_f = 0$ rad and a positive roll motion of $\phi_f = \frac{\pi}{2}$ rad to the floater. The pendulum starts at $\psi_p = 0$. The orientation of our system resulting from these imposed motions can be found in Figure 3.3.a.
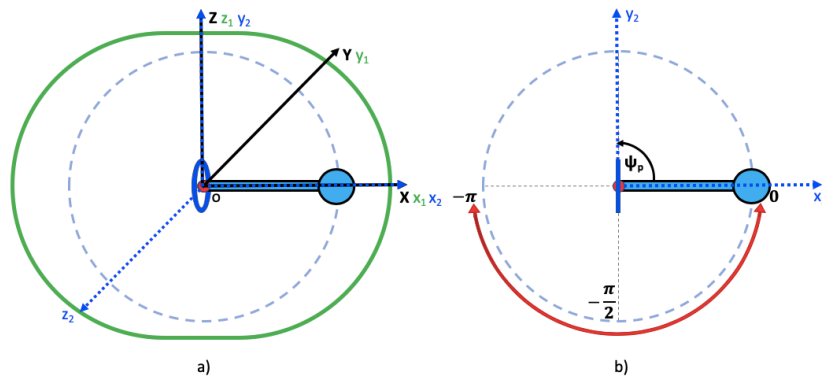
Figure 3.3: a). Orientation of the system after performing the imposed motions b). Expected rotation of the pendulum

In this particular case we expect the pendulum to perform an undamped negative rotation around the z_2-axis starting from 0 and ending to $-\pi$. Figure 3.4 shows us the results obtained from the numerical model, which are in accordance to our expectations.
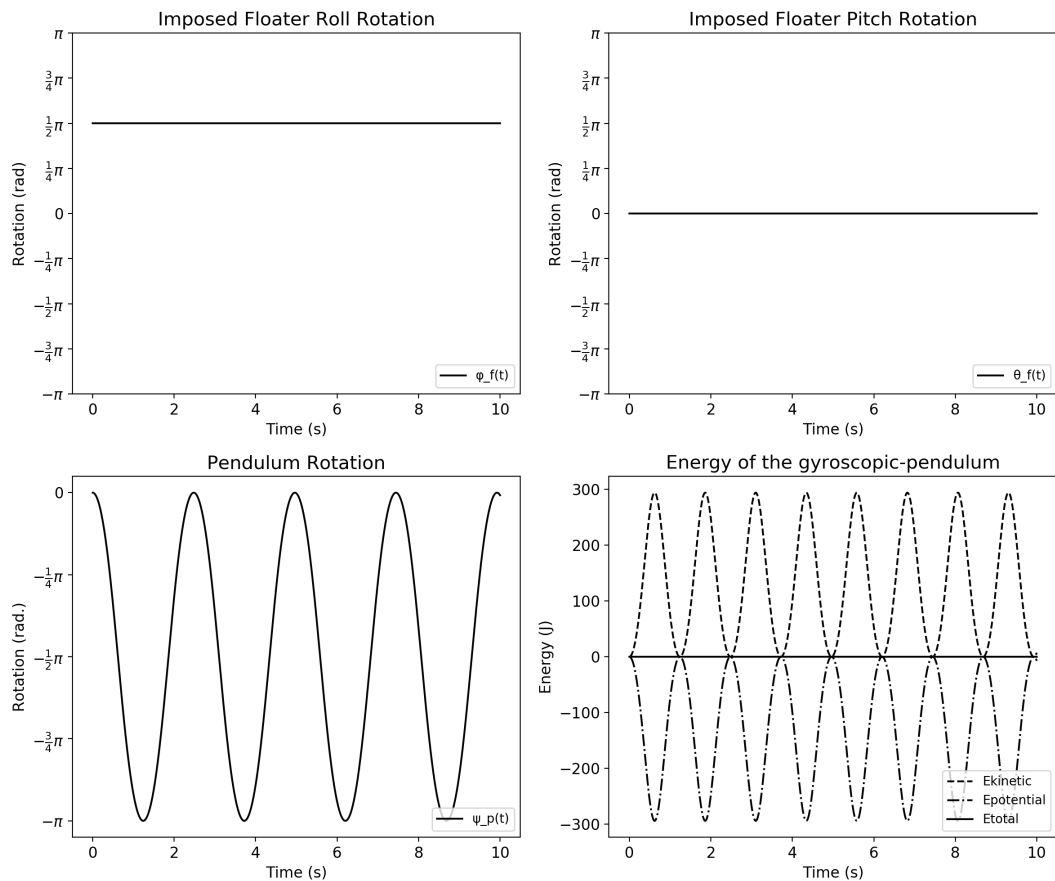
Figure 3.4: Results obtained from the numerical model

3.3.3. Imposed Positive Pitch and Positive Roll Motions

What happens if we perform two non-zero, but constant imposed motions? let us first impose a pitch rotation of $\theta_f = \frac{\pi}{2}$ rad and then a roll rotation of also $\phi_f = \frac{\pi}{2}$ rad. The pendulum starts at $\psi_p = 0$ rad.
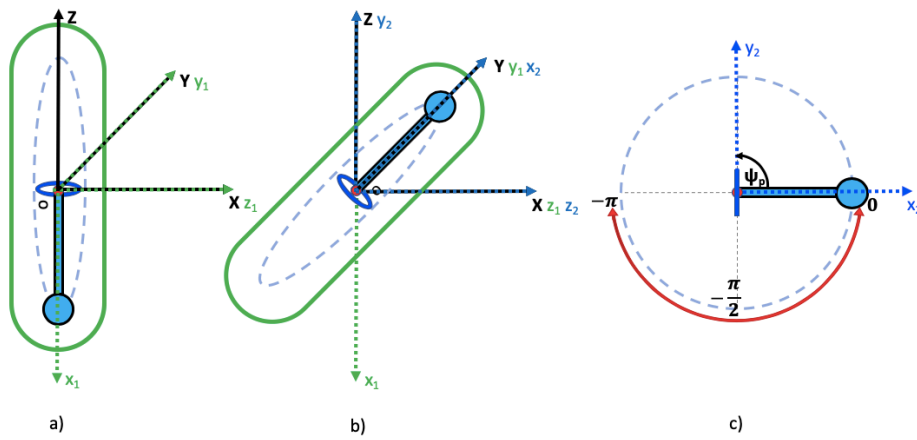
Figure 3.5: a).b). Orientation of the system after performing the imposed motions in order c) Expected rotation of the pendulum

Figure 3.5 gives us an overview of imposed rotations in correct order and our expected pendulum rotation. Our expectations are correct if we take a look at the results of the numerical model in Figure 3.6.
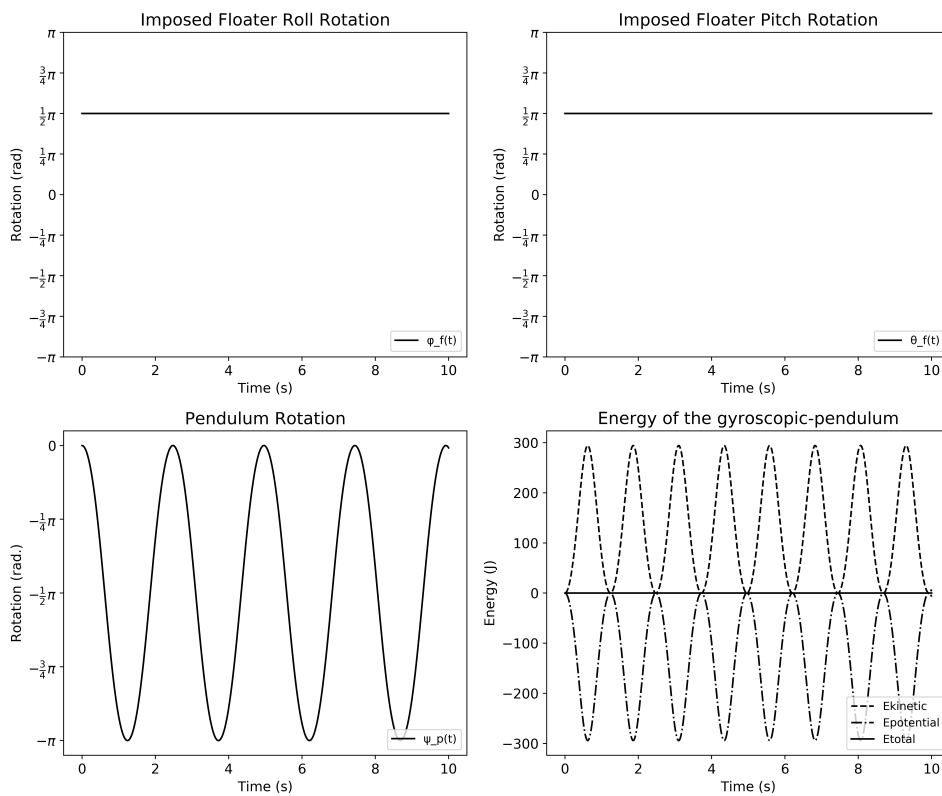
Figure 3.6: Results obtained from the numerical model

Based on the presented results, we can conclude that our mathematical model and numerical model are correct when we impose constant pitch and roll motions.

<div style="text-align: right">

4

</div>

<div style="text-align: right">

Hydrostatics

</div>

4.1. Introduction

In Chapter 3: Validation of the Model, we have shown that our mathematical and numerical models are correct for constant non-zero imposed motions. Since we imposed both pitch and roll motions, we did not have to introduce the inertia properties of our floater into the equations of motion.

In this chapter we will start with presenting a shape for the floater and introduce preliminary design values of our system. These preliminary design values will be used to compute the inertia properties of our systems, which are necessary to perform an initial stability check. After that we will present the stable position of both systems, which is basically a validation of the model without any imposed motions.

4.2. Floater Shape

Let us introduce a simple shape for the floater and compute the hydrodynamics. In Figure 4.1 a preliminary shape of the gyroscopic-pendulum is shown. The classical pendulum will have the same shape and dimensions as the gyroscopic-pendulum, but without the flywheel.
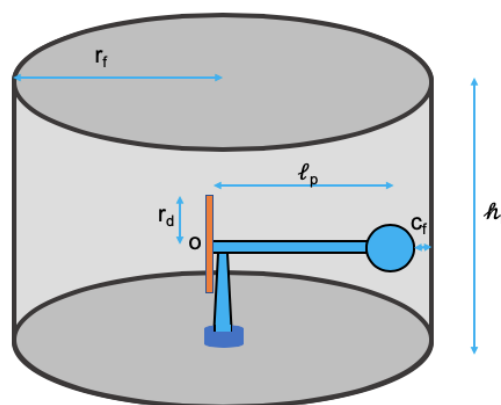
Figure 4.1: Preliminary design gyroscopic-pendulum device

We start off with introducing some values for the dimensions of the disk and pendulum, which are depicted in Figure 4.1. The numerical values we have chosen can be found in Table 4.1. From these dimensions we will compute all the necessary properties of our systems.

Parameter	Quantity [Unit]
Pendulum length, l_p	1 [m]
Pendulum mass, m_p	30 [kg]
radius disk, r_d	0.25 [m]
Thickness disk, t_d	0.10 [m]

Parameter	Quantity [Unit]
Density water, ρ_w	1050 [kg/m^3]
Density steel, ρ_s	7850 [kg/m^3]
Density acrylic glass, ρ_{acr}	1180 [kg/m^3]
Damping pendulum, c_p	0.106 [kg/s]
Damping disk, c_d	0.005 [kg/s]

Table 4.1: Initial dimensions pendulum and disk   Table 4.2: Constants

Table 4.2 shows the constants we will be using in our computations. Since the gravity of the earth and the presented densities don't need any explanation, let us discuss the damping coefficients for the pendulum and the disk. We assume the damping coefficient of the pendulum to be equal to the damping coefficient of the PTO. The damping of the disk will be assumed to be equal to air drag losses and bearing losses. For both coefficients, we will use the Doctoral thesis of Giovanni Bracco as our reference.[29].

4.3. Inertia Properties of the Systems

Inertia Properties of the Pendulum
Since we know the mass and length of the pendulum, we can compute its mass moment of inertia (assuming it to be a point mass).

$$I_p = m_p l_p^2 \tag{4.1}$$

Inertia Properties of the Disk
The disk will be made of steel, which has a density of ρ_s equal to 7850 $\frac{kg}{m^3}$. We can find the mass of the disk according the following equation:

$$\begin{aligned} m_d &= \rho_s V_d \\ &= \rho_s \pi r_d^2 t_d \end{aligned} \tag{4.2}$$

We can now compute the mass moment of inertia of the disk in all three directions.

$$Id = \frac{1}{2} m_d r_d^2$$

$$Id, x = Id, y = \frac{1}{4} m_d r_d^2 \tag{4.3}$$

Inertia Properties of the Floater
We have already introduced the shape of our floater, let us now state some practical requirements in order to find the its dimensions.

The floater will be made of acrylic glass, which is a light but strong plastic polymer with a density of ρ_{acr} equal to 1180 $\frac{kg}{m^3}$. Known industry can provide it with a maximum of thickness of 10 cm. This will be our preliminary design value for the thickness t_f of the floater. The pendulum and the disk should not be hindered when rotating inside the floater. We can state this requirement in form of two inequalities.

$$\begin{aligned} h_f &> 2r_d \\ r_f &> l_p \end{aligned} \tag{4.4}$$

We can easily satisfy both requirements by introducing a clearance c_f equal to 10 *cm* for both. Since the pendulum and the disk cannot translate in the x,y and z direction relative to the floater, we can write the following two expressions for h_f and r_f.

$$\begin{aligned} h_f &= 2r_d + 2c_f \\ r_f &> l_p + c_f \end{aligned} \tag{4.5}$$

We are now able to compute the mass and afterwards the mass moment of inertia of the floater, respectively in Equation 4.6 and Equation 4.7.

$$m_f = \rho_{acr}(h_f(\pi r_f^2 - \pi(r_f - t_f)^2) + \pi r_f^2 t_f) \tag{4.6}$$

$$I_f = \frac{1}{12}m_f(3(r_f^2 + (r_f - c_f)^2) + h_f^2) \tag{4.7}$$

Properties of the System

The total mass of our system is an important property for the calculations of the hydro-static stability. We have already presented the equations containing the computations of the masses of the pendulum, disk and floater , which enables us to compute the total mass of our system. The total mass of our system will also govern the draft of the floater. The expression of the total mass of our system can be found in Equation 4.8 and the expression for the draft can be found in Equation 4.9.

$$m_{tot} = m_p + m_d + m_f$$
$$m_p + \rho_s \pi r_d^2 t_d + \rho_{acr}(h_f(\pi r_f^2 - \pi(r_f - t_f)^2) + \pi r_f^2 t_f) \tag{4.8}$$

$$D_f = \frac{m_{tot}}{\rho_w \pi r_f^2} \tag{4.9}$$

Since all unknown properties depend only on the known variables, we can compute them by using the above equations. An overview of the numerical values of the gyroscopic-pendulum and the classical pendulum are shown in the table below.

Parameter	Gyroscopic-pendulum	Classical pendulum	[Unit]
Mass Moment of inertia pendulum, I_p	30	30	$[kgm^2]$
Mass of the disk, m_d	154.0	0.0	$[kg]$
Mass Moment of inertia Disk I_d	5.0	0.0	$[kgm^2]$
Floater clearance, c_f	0.10	0.10	$[m]$
Floater height, h_f	0.70	0.70	$[m]$
Radius floater, r_f	1.10	1.10	$[m]$
Thickness of the floater, t_f	0.10	0.10	$[m]$
Mass floater, m_f	994	994	$[kg]$
Mass moment of inertia floater, I_f	590	590	$[kgm^2]$
Total mass of the system, m_{tot}	1178	1023	$[kg]$
Draft floater, D_f	0.30	0.26	$[m]$

Table 4.3: Dimensions and properties of both systems

4.4. Stability of the Floaters

4.4.1. Initial stability

Our floating systems must be stable, which requires a metacentric height GM which is larger than zero for initial stability.

$$GM = KB + BM - KG > 0 \tag{4.10}$$

In which KG is the height of the floaters center of gravity above the keel, BM is the metacentric radius and KB is the distance between the center of buoyancy and the keel . Due to the shape of our system, computing GM is quite straightforward, see the expressions in Equation 4.11

$$GM = \frac{D_f}{2} + \frac{I_t}{\nabla} - \frac{h_f}{2}$$
$$= \frac{D_f}{2} + \frac{\frac{\pi}{4}r_f^4}{\pi r_f^2 D_f} - \frac{h_f}{2} \tag{4.11}$$
$$= \frac{D_f}{2} + \frac{r_f^2}{4D_f} - \frac{h_f}{2}$$

In which I_t is the moment of inertia of water plan area in m^4 and ∇ is the volume of displacement in m^3. Substituting numerical values provided in Table 4.3, we can compute the numerical values for GM for both systems.

- $GM_{gp} = 0.82m$

- $GM_{cp} = 0.96m$

Clearly the GM values for both systems are larger that zero, so we can assume to have two stable floating systems.

4.4.2. Hydrostatic Coefficients
Since we now know the the shape and dimensions of our system and its GM we can compute the hydrostatic stiffness and the damping term for the floater. Due to the symmetric shape of the floater, the hydrostatic stiffness and damping for both pitch and roll motions are assumed to be equal.

$$k_w = \rho_w g \nabla GM = \rho_w g \pi r_f^2 D_f GM \tag{4.12}$$

We can now find the rotational damping coefficient by assuming it to be equal to 1 percent of the critical damping coefficient.

$$c_w = 0.001 \sqrt{I_f k_w} \tag{4.13}$$

Parameter	Gyroscopic-pendulum	Classical Pendulum	[Unit]
Hydrostatic stiffness, k_w	9505	9618	$[kgm^2/s^2]$
hydrostatic damping, c_w	2.37	2.38	$[kgm^2/s]$

Table 4.4: Stiffness and damping coefficients of the systems

4.4.3. Stable Positions
Without imposing any motion to both systems and setting the initial conditions to zero, means that the pendulum is positioned in the x-direction with a distance of l_p from O. We can now imagine the floater to pitch a little amount in the positive direction as a result to the gravity force due to the mass of the pendulum. Since we have introduced a damping in our system, this motion must be a decaying oscillation and since we also have introduced a hydrostatic stiffness coefficient it must also approach a stable pitch angle.

Let us now try to find this stable positions of our systems by considering the static equilibrium of our systems. This requires us to set all the velocity and acceleration terms in the equation of motion of the pitch equal to zero, resulting in Equation 2.5.

$$k_w \theta_f - cos(\psi_p)cos(\theta_f)cos(\phi_f)m_p g l_p = 0 \tag{4.14}$$

We know that at the initial conditions $\psi_p = \phi_f = 0$, so we end up with the following equation for both systems:

$$\theta_f - \frac{m_p g l_p}{k_w} cos(\theta_f) = 0 \tag{4.15}$$

This equation is true for $\theta_f = 0.031 \; rad$ for both systems.

Let us now find the stable positions of our systems from the numerical model. We can do this by just running our scripts without any imposed motion, without an applied torque and all initial values equal to zero. The results are shown in Figure 4.2.
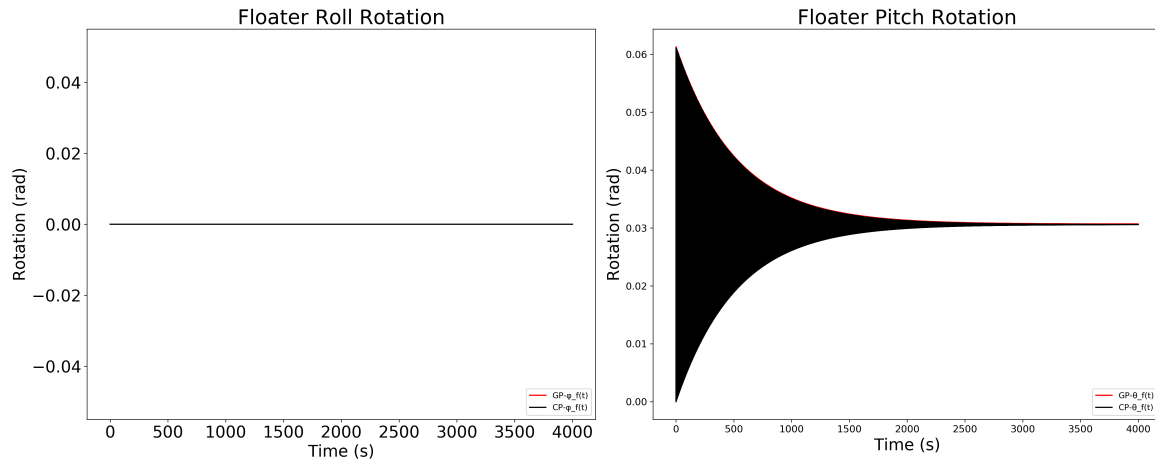
Figure 4.2: Stable positions of both systems

The two graphs depict the roll and pitch motions of both floaters and indeed, as expected, the floaters starts pitching in the positive direction and approaches a stable position of approximately $\theta_f = 0.03 \; rad$.

5

Power Efficiency

5.1. Introduction

In Chapter 4: Hydrostatics, we have introduced the shape of our systems and their dimensions. In this chapter we perform numerical tests on our systems to provide an answer to our research question.

We start with discussing the manner we impose motions to our system and continue with explaining the applied torque on the disk. We then explain the way we approximate the average power inputs and outputs of the systems. Eventually the results in terms of ratios between the power efficiency of both systems are shown at the end of this chapter.

5.2. Numerical Simulation

5.2.1. Imposed Motion

Our device will be operating nearshore and generate electricity from the motions of the waves. We are clearly interested in the net electricity output of this system and should perform simulations to get an overview of the power output.

The most accurate manner to find the power output of our system would be by simulating waves based on a wave spectrum from the location of interest and find the response of our dynamical system on these waves in terms of RAO's. However this is a quite complex operation that requires us to have the correct (and final) shape of our device which is beyond the scope of this report.

Instead we directly impose certain motion in the incoming wave direction and observe the floater response in the other direction. Since we are in a very preliminary phase of the research, we will be only imposing a simple harmonic roll motion to the floater in this report. The amplitude and frequency range of this motion is directly taken from the met-ocean data in North East Java sea, which can be found in Table 5.1

Parameter	Quantity Range [Unit]
Water Depth, h	5.39 - 62.10 [m]
Period, T_p.	3.60 - 6.54 [m]
Frequency, f_p	0.95 - 1.75 [rad/s]
Wave Height, H_s	0.54 - 1.91 [m]
Wave length, L	15.95 - 54.09 [m]

Table 5.1: Wave Data (for 1 Year Return Period), location in North East Java, Indonesia [33]

An example of an imposed motion can be found Figure 5.1.
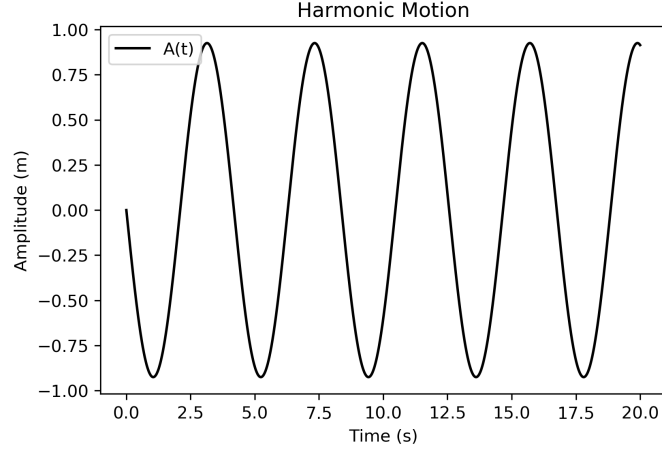
Figure 5.1: Imposed motion, H =1.75 m and ω = 0.75 rad/s

5.2.2. Applied Torque to the Disk

Besides the imposed motion, we also provide a certain torque to the flywheel. The torque can be found by multiplying the mass moment of inertia of the disk I_d with the angular acceleration of the disk α_d. In our numerical model, the torque will only be applied in a certain period of time t_{trq} to achieve a certain target velocity w_d in that period of time. Equation 5.1 provides us the expression we use to define the torque in our numerical system.

$$T = I_d \frac{\omega_d}{t_{trq}} \qquad\qquad for\ t\ < t_{trq} \qquad\qquad (5.1)$$

In which T is the applied torque in Nm, I_d is the mass moment of inertia of the disk around it's own COG in kgm^2 , ω_d is the targeted angular velocity of the disk in $\frac{rad}{s}$ and t_{trq} is the duration of the applied torque in $seconds$.

We will apply different torques to the flywheel and see how it will affect the average power output of the pendulum. An overview of the applied torques can be found in Table 5.2.

ω_d [rad/s]	t_{trq} [s]	T [Nm]
10	20	2.5
20	20	5
30	20	7.5
40	20	10

Table 5.2: Overview applied torque cases

5.2.3. Power of the System
Energy Input
We impose harmonic motions to our system, which means we put power in the system. Since we have kind of assumed an RAO of 1, the average power of the imposed motion is equal to the average power contained in the waves which have the same properties as the imposed motions. Assuming deep water condition, we can find the time-averaged power per meter wave crest in linear waves as follows[34].

$$P_w = \frac{1}{32\pi}\rho_w^2 gTH^2 \qquad\qquad (5.2)$$

In which P_w is the power per meter width in $\frac{W}{m}$, T is the wave period in s and H is the wave height in m. However, we are interested in finding the power of the imposed motions based

on the dimensions of our system, so we need to multiply this expression with the width of our structure. This results in the following equation, which we will use in our computation.

$$P_w = \frac{1}{32\pi}\rho_w g^2 T H^2 2r_{fl} \tag{5.3}$$

The gyroscopic-pendulum is the only model that has energy input in form of the applied torque. We approximate the energy input to the disk as the applied torque times the total amount of rotation of the disk when this torque is applied.

$$E_d = T\phi_d \tag{5.4}$$

In which ϕ_d is disk position in radian evaluated at the last time step when the torque is applied.

We can now find the average input power to the disk by dividing the Energy input by the total amount of simulation time.

$$P_d = \frac{E_d}{t_s} \tag{5.5}$$

In which P_d is the average power input to the disk in W and t_s is the simulation time in *seconds.*

Power Output
We have introduced an damping term in the equations of motion of the pendulum to represent the PTO for both gyroscopic-pendulum and classical pendulum systems. The amount of power we can obtain from our systems, depends on this damping term and the velocity of the pendulums.

$$P = C_p \dot{\psi}_p^{\;2} \tag{5.6}$$

In our numerical model, the angular velocity of the pendulums $\dot{\psi}_p$ is an array, so if we use the mean function in Python, we will get the average power output of both systems.

5.2.4. Simulation Conditions and Output
To make sure we have fair comparison between different inputs and outputs, we have to perform the numerical simulations in the same conditions. All tests will have the following properties:

- Simulation time = 3600 s
- Number of time steps 36000

The resolution used for the amplitude range is 0.075 m per step, while the resolution of the frequency range is equal to 0.05 rad/s per step. So the amplitude range is covered by 19 steps and the frequency range is covered by 17 steps. This results in $19 * 17 = 323$ measurement points for our graphs.

We are interested in the power efficiency of the gyroscopic pendulum relative to the power efficiency of the classical pendulum and consider this as the output of our numerical model. The efficiency for the gyroscopic-pendulum and the classical pendulum can be computed as according to Equation 1.7 and Equation 1.8.

$$\eta_{gp} = \frac{P_{gp} - P_{d,in}}{P_{m,in}} \tag{5.7}$$

$$\eta_{cp} = \frac{P_{cp}}{P_{m,in}} \tag{5.8}$$

In which, P_{gp}, $P_{d,in}$ and $P_{m,in}$ are respectively the average power output of the gyroscopic-pendulum, the average power input to the disk and the average power input of the imposing motions in $Watt$.

5.3. Results

5.3.1. Gp Without Applied Torque vs Cp

Let us first of all compare the gyroscopic-pendulum and the classical pendulum without any applied torque to the first one. Both systems will have the same imposed motions and the aim is to see whether the gyroscopic-pendulum out performs the classical pendulum already based on the existence of the disk. Figure 5.2 shows an contour plot of the power efficiency ratio of the gyroscopic-pendulum and the classical pendulum. The horizontal axis consists of the frequency range of the imposed motions in $\frac{rad}{s}$ and the vertical axis consists of the amplitude range of the imposed motions in m.
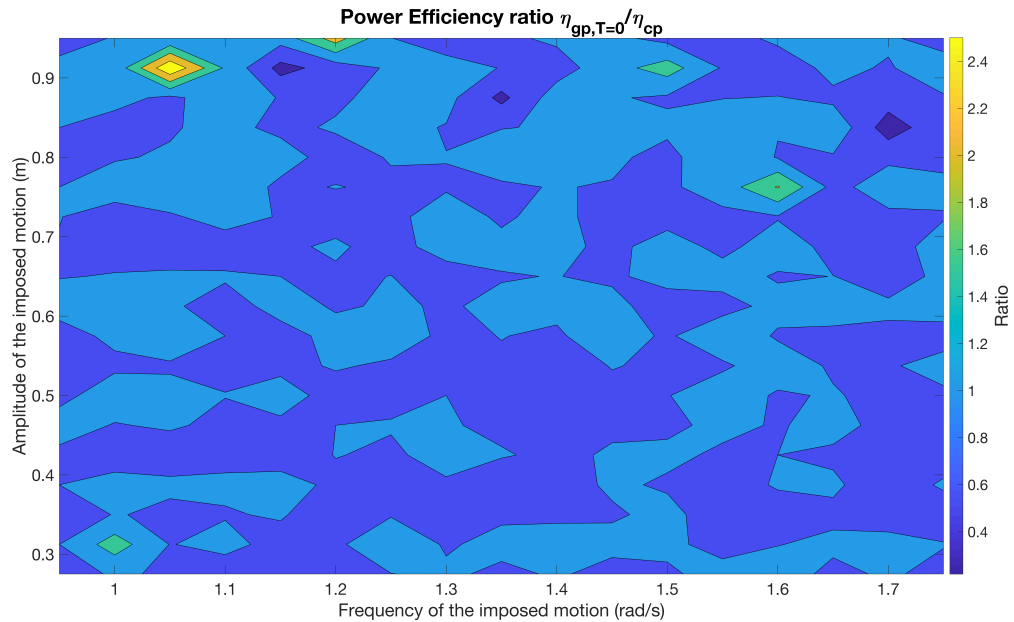
Figure 5.2: Gyroscopic-pendulum vs classical pendulum without power input to the disk

It can be seen that for most parts of the frequency and amplitude ranges, the power efficiency ratio is either well below 1 (dark blue color) or a little bit bigger than 1 (light blue color). An ratio below 1, implies that the cp is outperforming the gp, a ratio of 1 means that the performance is the same and a ratio above 1 means that the gp is outperforming the cp.

The contour plot shows us that the performance of both systems is quite close to each other. Only at a few spots, the gp is significantly outperforming the cp. These spots are around $(\omega_m = 1.05, A_m = 0.9)$ and $(\omega_m = 1.45 - \omega_m = 1.6, A_m = 0.75)$.

5.3.2. Gp With Applied Torque vs Gp Without Applied Torque

Before we go to comparing the gyroscopic-pendulum with applied torque to the classical pendulum, we will compare the gyroscopic-pendulum with applied torque to the itself without applied torque. If we can observe significant increases efficiency ratios, we can be sure that it comes from the gyroscopic effect.

The results can be found in Figure 5.3. We can see clearly significant decreases and increases of the efficiency ratios. The decreases can be found in the lower ranges of frequency and amplitude, while the increases can be seen in the higher ranges of frequency and amplitudes.
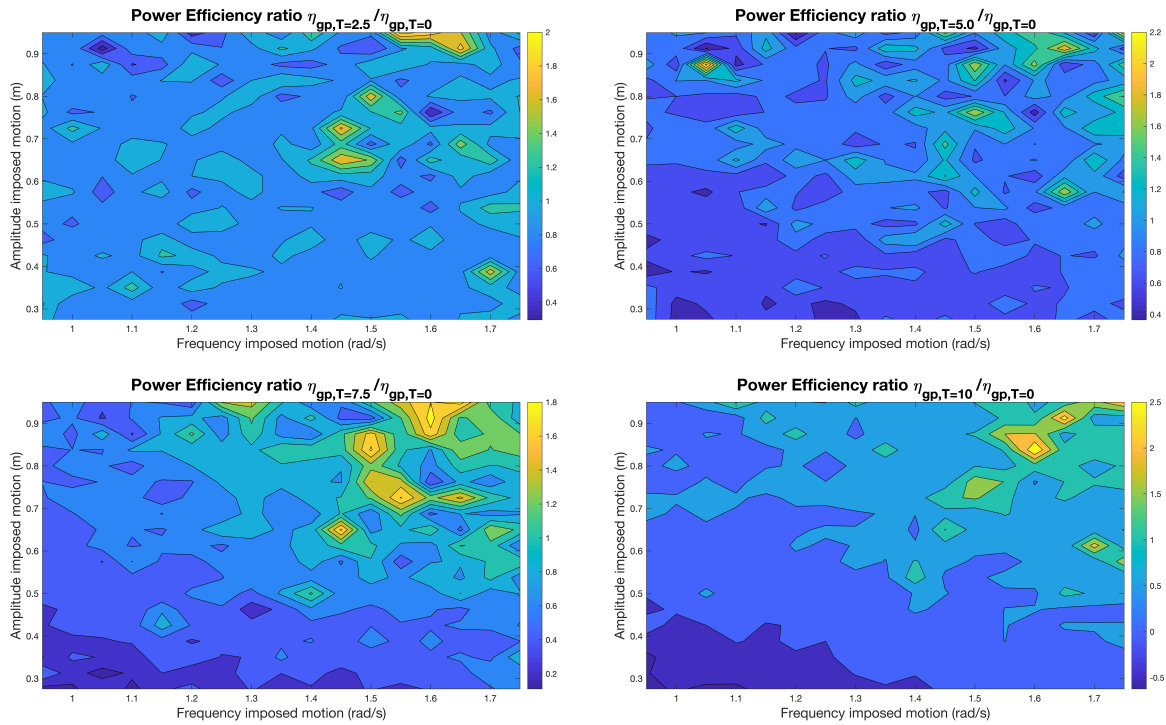
Figure 5.3: Gyroscopic-pendulum with four cases of applied torque vs the
gyroscopic-pendulum without applied torque

5.3.3. Gp With Applied Torque vs Cp

Let us now compare the gyroscopic-pendulum to the classical pendulum while we apply the distinct torque cases, shown in Table 5.2, to the flywheel. The aim is to see the effect of the flywheel on the power output compared to the classical pendulum. Figure 5.4 shows us four contour plots of the efficiency ratio between the test cases.

The top left plot shows the ratio of the case where the applied torque is equal to 2.5 Nm. We can see that due to the power input to the torque, the efficiency ratio is a bit below 1 for the largest part of the amplitude and frequency ranges. We can also see some scatter, where the ratio is equal to 1.0. In the frequency range of 1.4 to 1.7 $\frac{rad}{s}$ combined with the amplitude ranges of 0.65 to 0.95 m, we can see ratios significantly above 1.0.

The top right plot shows the efficiency ratio when the applied torque is increased to 5 Nm. Now we can clearly see that in the lower ranges of amplitude and frequency of the imposed motions, the ratio is well below 1.0. If take a look at the higher ranges of amplitude and frequency, we start to see some scatter of increasing efficiency ratio. However the areas of these points, in terms of frequency times the amplitude, are smaller than the previous case.

The bottom left plot shows the results of the third case. In this case we can see kind of linear contours between emerging zones. In the bottom we can see a zone in which the ratio is approximately equal to 0.4, followed by another zone which consists of a ratio around 0.6. The third zone has a ratio of 0.8 and the fourth zone has a ratio of 1.0. The last zone, we can see significant ratio increases from 1.2 up to 2.2.

The bottom right plot depicts the results of the fourth case. We can see the pattern become more visible. In this case we can see negative values for the efficiency, which implies that there are combinations of imposed motions and applied torque in which the average power input to the disk is larger than the average power output of the pendulum. We can also see that areas in which the efficiency ratio is larger than 1.0, are now smaller than the previous case. However, the maximum of the ratio has increased to 3.0 compared to 2.2 of the third case.
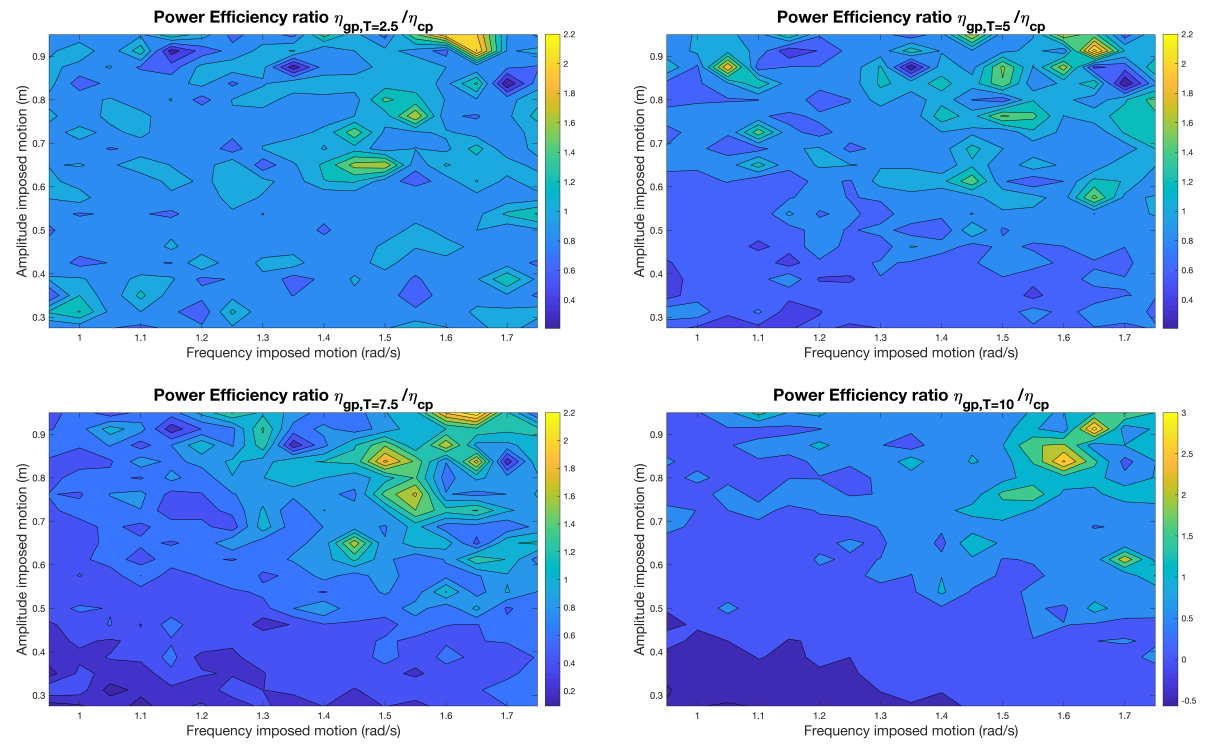
Figure 5.4: Gyroscopic-pendulum with four cases of applied torque vs the classical pendulum

5.3.4. Detailed Analysis

In the previous subsections, we have discussed the power efficiency ratios, let us now analyse the dynamics of our system for two points in an interesting area in our contour plots shown in Figure 5.4. The interesting area is the top right area of the contour plots, since we can see significant ratio increases in that region. That area becomes even more interesting because very close to these high ratios, we can also see a small area of quite low ratios. This small area can be found in all four cases and consists of the lowest ratio around 0.25 at the coordinate (1.7, 0.8375). To dive a bit deeper, we will compare the motions of our systems for this point and the point which gives us the maximum ratio in that region. Let us make the comparison from the contour plot of the fourth case, in which the applied torque is equal to $10\ Nm$. Figure 5.5 shows the motions of our systems when the efficiency ratio is maximum in the fourth test case, while Figure 5.6 depicts the motions of our system for the low ratio discussed above.
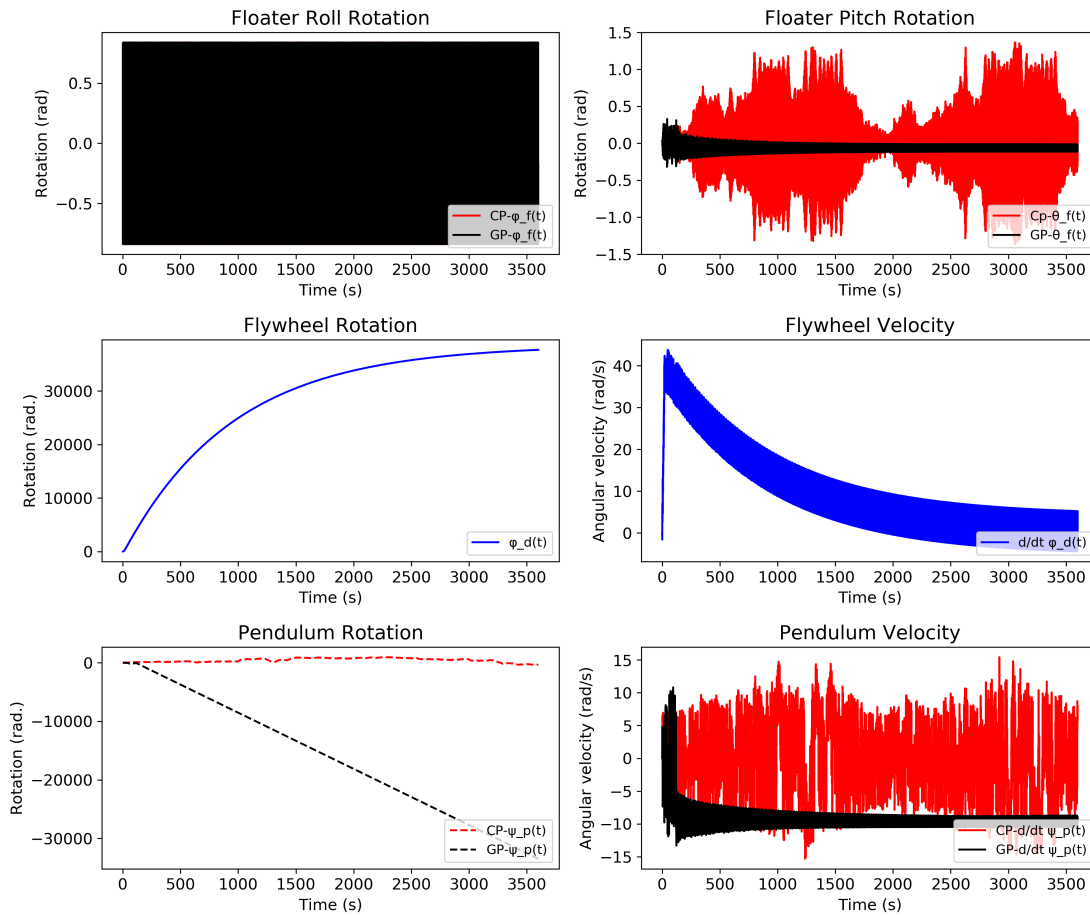
Figure 5.5: Response of the systems for imposed motion with $\omega_m = 1.6\ rad/s$, $a_m = 0.84\ m$ and $T = 10\ Nm$

The figure consists of six subplots of which the titles tell us what motion is depicted. The difference between the pendulum rotation and velocity of the cp and the pendulum rotation and velocity of the gp stands out immediately. The relatively constant and relatively high velocity of the pendulum of the gp system causes very small floater pitch rotations to the gp systems compared to the cp system.

Furthermore, the decay of the flywheel velocity from the target velocity is quite fast, which implies that the flywheel properties are not optimized yet.

In short, we can see that the high average power output of the gyroscopic-pendulum is caused

by the high and constant velocity of the pendulum, which in turn is the result of high average power input to the disk.

Let us now discuss the responses of the systems which result in a very low efficiency ratio, see Figure 5.6. We can now see the opposite phenomena occur. In this case the pendulum rotation of the cp system is much higher and has and steep constant increase in time, while the pendulum rotation of the gp system is very low and almost no increase after a certain amount of time. The velocity of the pendulum of the cp system is now relatively high and constant relative to the pendulum velocity of the gp system. The pitch motion of the cp system is much smoother and more constant than the one of the gp system. The flywheel shows somewhat the same behaviour, except the fact that it has more irregular oscillation in its velocity in the case of high efficiency ratio.
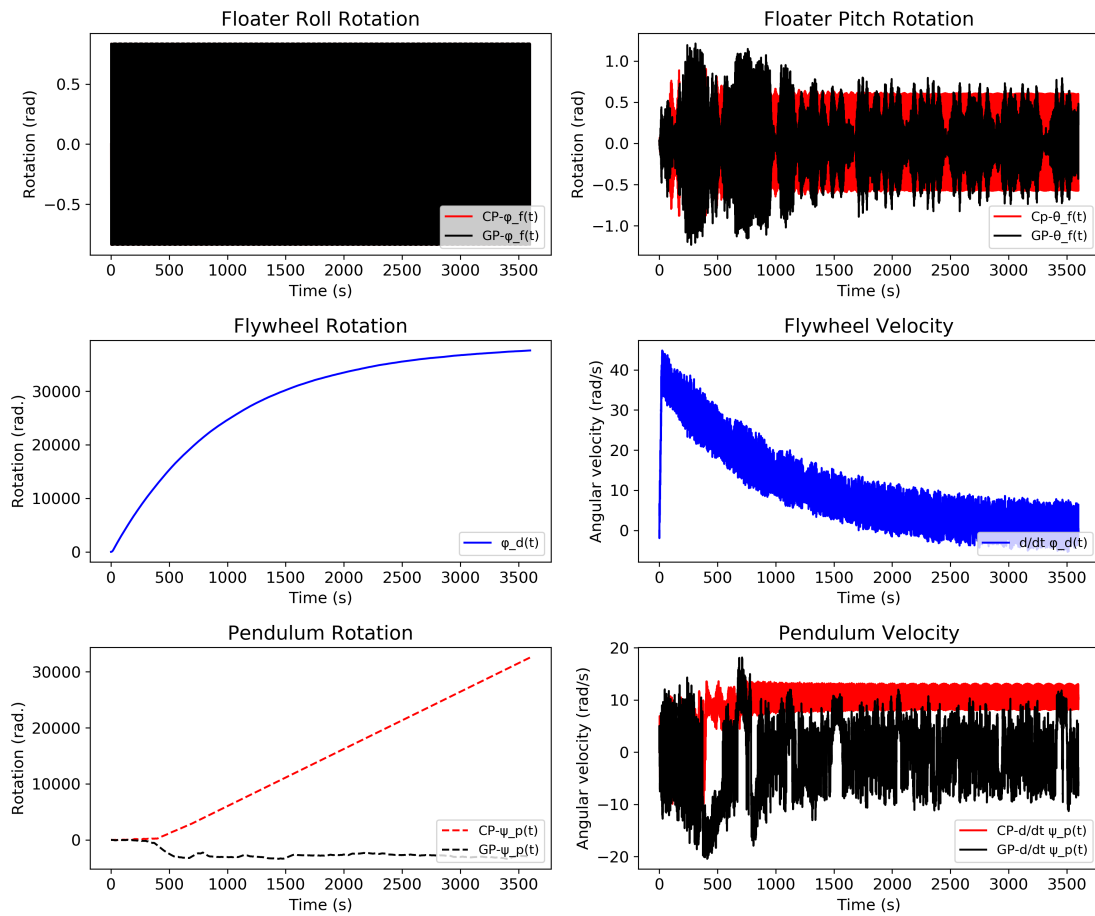
Figure 5.6: Response of the systems for imposed motion with $\omega_m = 1.7\ rad/s$, $a_m = 0.84\ m$ and $T = 10\ Nm$

6

Conclusion and Recommendations

6.1. Introduction
In this chapter we will try to formulate our conclusions based on the results we have obtained in chapter 5: Power Efficiency. Eventually we want to provide a validated answer to our research question.

We will start with our conclusions based on the presented tests and results. After that we will give an direct answer to our research question. We will end this chapter and this report with some recommendations for further research and development of the gyroscopic-pendulum.

6.2. Conclusion
Let us now present the conclusions we can make based on the numerical results.

Gp Without Applied Torque vs Cp
Our first test was to show whether the comparison between gp and the cp is fair to make. We can see that the gyroscopic-pendulum (gp) without a power input has a quite similar performance, in terms of average power output, as the classical vertical axis pendulum (cp). So, we can conclude that we are making a fair comparison between the two systems.

Gp With Applied Torque vs Gp Without Applied Torque
We have also performed a comparison between the gyroscopic-pendulum with the applied torques and the gyroscopic-pendulum without the applied torques. The aim was to show that any efficiency increase in this test must originate from the gyroscopic-effect. Based on the obtained results, we can conclude that at certain zones, the gyroscopic effect is the only reason for the increased average power output and thus increased efficiency.

Gp With Applied Torque vs Cp
Our final test and the most important one is meant to see whether the gp system results in an improved average power output relative to the cp. Based on the results, we can conclude that at certain zones in terms of frequency and amplitude ranges, the gp is indeed outperforming the cp.

Furthermore, based on the detailed analysis, we can conclude that regular harmonic response of the floater pitch motion results in more and linearly increasing rotations of the pendulum. This implies that the velocity of the pendulum is characterized by simple harmonic oscillation around a relatively high velocity. Eventually it results in higher average power output and thus higher efficiency ratio compared to the classical pendulum.

Answer to the Research Question

We have now come to a very important part of this report. Let us once again present the research question of this report:

in which ranges of amplitude and frequency of an imposed motion to the floater does the gyroscopic-pendulum result in an improved average power efficiency compared to a classical vertical-axis pendulum?

The answer to this question based on our results obtained from the numerical simulations is as follows:

The gyroscopic-pendulum has a higher efficiency compared to the classical VAP pendulum when the frequency of the imposed motion is in the range of 1.4 to 1.75 $\frac{\text{rad}}{\text{s}}$ and the amplitude is in the range of 0.6 to 0.95 m.

6.3. Recommendations

Based on the obtained results and encountered issues, several recommendations will be formulated.

- The mathematical models for the cp and gp are consisting of 3 and 4 DOF respectively, while in reality this should be 7 and 8 DOFs. So it is recommended to derive the equations of motions including the surge, sway and heave motions to obtain a more realistic model for both systems.

- The precessional motion is very sensitive to the mass moment of inertia of the disk. We can see from the results that velocity of the flywheel, even though it has a very low damping coefficient, decays quite fast. Hence it is sensible to search for the optimum mass moment of inertia of the disk to make sure the decaying characteristic of the velocity is improved.

- The decaying characteristic of he flywheel can be counteracted by introducing a control mechanism to the disk. The control mechanism should be capable of providing the minimum amount of power to counteract the decay of the disk velocity due to the damping.

- The results we have obtained are based on a simulation time of 1 hour (3600 seconds). The systems might need more time to achieve steady state. It is recommended to perform tests under a much longer simulation time.

- The starting dimensions of the disk and pendulum are chosen to be some realistic numbers, but a thorough dimension analysis could result in optimal dimensions.

- We have imposed simple harmonic motions to our system, while in reality non-linear incoming waves result in the response of our system. It is recommended to perform hydrodynamic analysis of the systems and impose waves in form of force, instead of imposing motions.

Bibliography

[1] *ADOPTION OF THE PARIS AGREEMENT*, Framework Convention on Climate Change, 2015. United Nation.

[2] D.P. Vuuren, P.A. Boota. The implications of the Paris climate agreement for the Dutch climate policy objectives. Technical report, PBL Netherlands Environmental Assessment Agency, 2017.

[3] International Energy Agency. *World Energy Outlook 2018.* doi: {https://doi.org/https://doi.org/10.1787/weo-2018-en}. URL `https://www.oecd-ilibrary.org/content/publication/weo-2018-en`.

[4] ExxonMobil. *2018 Outlook for Energy: A view to 2040.* 2018. URL `https://corporate.exxonmobil.com/en/~/media/Global/Files/outlook-for-energy/2018-Outlook-for-Energy.pdf`.

[5] European Commission. Renewable Energy Directive. 2018. URL `https://eur-lex.europa.eu/legal-content/EN/TXT/PDF/?uri=CELEX:32009L0028&from=EN`.

[6] Renewable Energy Policy Network for the 21st Century. *RENEWABLES 2018 GLOBAL STATUS REPORT.* 2018. URL `http://www.ren21.net/gsr-2018/`.

[7] International Renewable Energy Agency. *Renewable energy highlights 2018.* 2018. URL `http://www.ren21.net/gsr-2018/pages/highlights/highlights/`.

[8] International Energy Agency. *Renewables 2018.* IEA Publications, 2018. URL `https://www.iea.org/renewables2018/`.

[9] International Energy Agency. *Offshore Energy Outlook.* IEA Publications, 2017. URL `https://www.iea.org/renewables2018/`.

[10] T.Todorcevic. Power Electronic Converter for an Electroactive Polymer-based Wave Energy Harvester. 2018. doi: {https://doi.org/10.4233/uuid:c0ddf71c-b8a5-42aa-96da-85defe259115}.

[11] Davide Magagna,Riccardo Monfardini,Andreas Uihlein. JRC Ocean Energy Status Report 2016 Edition. Technical report, 2016. URL `http://publications.jrc.ec.europa.eu/repository/handle/JRC104799`.

[12] Ocean Energy Europe. Ocean energy project spotlight Investing in Tidal and Wave Energy, 2017.

[13] Simeec Atlantis Energy. Tidal stream project MeyGEn. -, 2019. URL `https://simecatlantis.com/projects/meygen/`.

[14] Atlantis Resources. AR1500 TIDAL TURBINE, 2019.

[15] N. Pozzi, G. Bracco, S.A. Sirigu, G. Mattiazzo. PeWEC: Experimental validation of wave to PTO numerical model. *Elsevier*, 2018.

[16] He, Hongzhou and Qu, Quanyou and Li, Juyue. Numerical Simulation of Section Systems in the Pelamis Wave Energy Converter. *Advances in Mechanical Engineering*, 5: 186056–186056, 01 2015. doi: {10.1155/2013/186056}.

[17] Antonio F.O Falcao. Modeling of Wave Energy Conversion. *Universidade Tecnica de Lisboa*, 2014.

[18] L.M. Masturi, H. Hendrikse, A.J.Laguna, A.V. Metrikine. Gyroscopically enhanced vertical axis pendulum for wave energy conversion. *WDD,* 2019.

[19] European Marine Energy Centre. PELAMIS WAVE POWER. -, 2019.

[20] T. Adrinto, H. Li. Ocean Wave Energy Converters: Status and Challenges. 2018. doi: {https://doi.org/10.3390/en11051250}.

[21] E.M. Dolores, S.LG. Jos,N. Vicente. Classification of Wave Energy Converters. *Recent Adv Petrochem Sci*, 2017.

[22] Ye Li, Yi-Hsiang Yu. A Synthesis of Numerical Methods for Modeling Wave Energy Converter-Point Absorbers. *Renewable and Sustainable Energy Reviews*, 5 2012.

[23] AW-Energy. WaveRoller. -, 2019. URL https://aw-energy.com/waveroller/.

[24] Ocean Energy Systems. ANNUAL REPORT AN OVERVIEW OF OCEAN ENERGY ACTIVITIES IN 2017. -, 2007.

[25] Parmeggiani, Stefano and Kofoed, Jens and Friis-Madsen, Erik. Experimental Study Related to the Mooring Design for the 1.5 MW Wave Dragon WEC Demonstrator at DanWEC. *Energies*, 6:1863–1886, 04 2013. doi: {10.3390/en6041863}.

[26] Poullikkas, Andreas. Technology prospects of wave power systems. *Electronic Journal of Energy & Environment*, pages –, 01 2014.

[27] Heller, Valentin and Member, Iahr and Chaplin, John and Farley, Francis and Hann, Martyn and Hearn, G.E. Physical model tests of the anaconda wave energy converter. pages –, 03 2010.

[28] Battezzato, Alessandro and Bracco, Giovanni and Giorcelli, Ermanno and Mattiazzo, G. Performance assessment of a 2 DOF gyroscopic wave energy converter. *Journal of Theoretical and Applied Mechanics*, 2015.

[29] Giovanni Bracco. ISWEC: a Gyroscopic Wave Energy Converter. *Porto Institutional Repository*, pages –, 05 2010.

[30] J.S. Brar, R.K. Bansal. A Texbook of Theory of Machines. -, 2010.

[31] Douglas Cline. Variational Principles in Classical Mechanics. *University of Rochester River Campus Libraries*, 2017.

[32] Thor I. Fossen. *Handbook of Marine Craft Hydrodynamics and Motion Control.* -, 2011. ISBN 9781119991496,9781119994138.

[33] Andojo Wurjanto. Metocean Data Integration Study for WMO Field. 2013.

[34] Joris van der Jagt. A methodology for assessing power performance of Wave Energy Converters, applied to a quasi-rigid submerged pressure differential device, 2018.